Article

Neuron

A Selectivity Filter Gate Controls Voltage-Gated Calcium Channel Calcium-Dependent Inactivation

Graphical Abstract

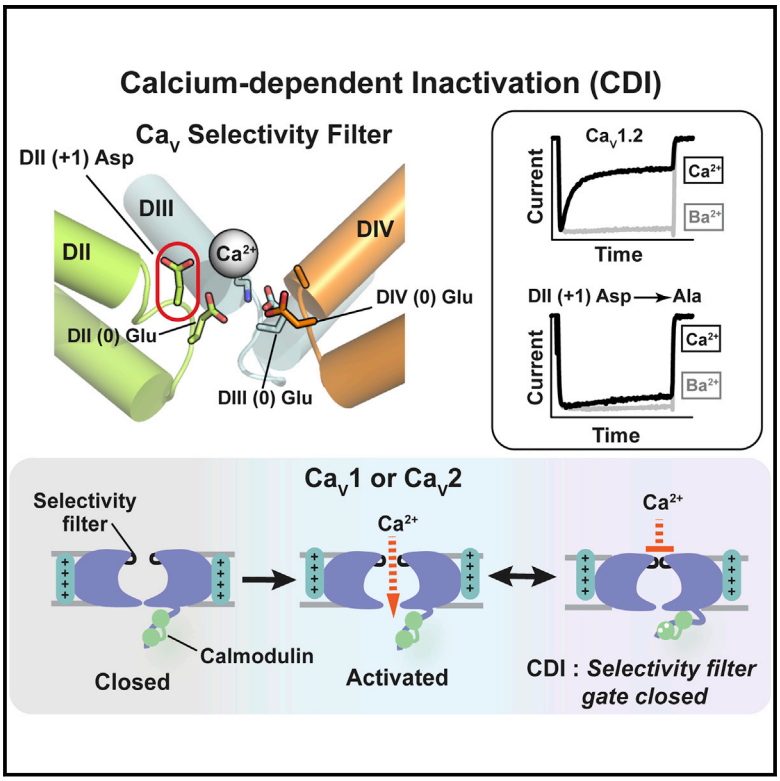

Highlights

- Ca_V selectivity filter forms the calcium-dependent inactivation (CDI) endpoint
- Conserved Ca_V domain II selectivity filter (+1) aspartate plays an active role in CDI
- Ca_V selectivity filter asymmetry is important for CDI
- Ca_Vs gating relies on an SF-based gating framework shared among the VGIC superfamily

Authors

Fayal Abderemane-Ali, Felix Findeisen, Nathan D. Rossen, Daniel L. Minor, Jr.

Correspondence

daniel.minor@ucsf.edu

In Brief

Calcium-dependent inactivation (CDI) is essential for voltage-gated calcium channel (Ca_V) autoregulation. Abderemane-Ali et al. demonstrate that the Ca_V selectivity filter (SF) forms the CDI gate, suggesting an SF-based inactivation paradigm shared with other voltage-gated ion channel (VGIC) superfamily members.

Abderemane-Ali et al., 2019, Neuron *101*, 1134–1149
March 20, 2019
https://doi.org/10.1016/j.neuron.2019.01.011

CellPress

CellPress

Neuron
Article

A Selectivity Filter Gate Controls Voltage-Gated Calcium Channel Calcium-Dependent Inactivation

Fayal Abderemane-Ali,[1] Felix Findeisen,[1] Nathan D. Rossen,[1] and Daniel L. Minor, Jr.[1,2,3,4,5,6,*]
[1]Cardiovascular Research Institute, University of California, San Francisco, San Francisco, CA 93858-2330, USA
[2]Departments of Biochemistry and Biophysics, and Cellular and Molecular Pharmacology, University of California, San Francisco, San Francisco, CA 93858-2330, USA
[3]California Institute for Quantitative Biomedical Research, University of California, San Francisco, San Francisco, CA 93858-2330, USA
[4]Kavli Institute for Fundamental Neuroscience, University of California, San Francisco, San Francisco, CA 93858-2330, USA
[5]Molecular Biophysics and Integrated Bio-imaging Division, Lawrence Berkeley National Laboratory, Berkeley, CA 94720, USA
[6]Lead Contact
*Correspondence: daniel.minor@ucsf.edu
https://doi.org/10.1016/j.neuron.2019.01.011

SUMMARY

Calcium-dependent inactivation (CDI) is a fundamental autoregulatory mechanism in Ca_V1 and Ca_V2 voltage-gated calcium channels. Although CDI initiates with the cytoplasmic calcium sensor, how this event causes CDI has been elusive. Here, we show that a conserved selectivity filter (SF) domain II (DII) aspartate is essential for CDI. Mutation of this residue essentially eliminates CDI and leaves key channel biophysical characteristics untouched. DII mutants regain CDI by placing an aspartate at the analogous SF site in DIII or DIV, but not DI, indicating that Ca_V SF asymmetry is key to CDI. Together, our data establish that the Ca_V SF is the CDI endpoint. Discovery of this SF CDI gate recasts the Ca_V inactivation paradigm, placing it squarely in the framework of voltage-gated ion channel (VGIC) superfamily members in which SF-based gating is important. This commonality suggests that SF inactivation is an ancient process arising from the shared VGIC pore architecture.

INTRODUCTION

Voltage-gated calcium channels (Ca_Vs) are multisubunit, macromolecular complexes that control cellular calcium entry in response to membrane potential changes in the brain, nervous system, and heart (Catterall, 2011; Zamponi et al., 2015). Due to the central role of calcium in cellular signaling (Clapham, 2007) and the importance of Ca_Vs as sources of Ca^{2+} influx that impact synaptic transmission, hormone release, vascular tone, muscle contraction, and gene expression (Nanou and Catterall, 2018; Simms and Zamponi, 2014; Zamponi et al., 2015), a multifaceted set of activity-dependent feedback regulation mechanisms shape Ca_V function. Chief among these is calcium-dependent inactivation (CDI), a process by which Ca^{2+} influx through Ca_V1 and Ca_V2 channels causes a cessation of ion conduction (Ben-Johny and Yue, 2014; Christel and Lee, 2011; Dunlap, 2007; Simms and Zamponi, 2014). Perturbations in CDI are involved in autism (Limpitikul et al., 2016), blindness (Singh et al., 2006), and cardiac arrhythmias (Alseikhan et al., 2002; Dick et al., 2016; Limpitikul et al., 2014, 2017; Mahajan et al., 2008; Morotti et al., 2012; Splawski et al., 2004, 2005), demonstrating that CDI is an important factor in diseases linked to Ca_V dysfunction.

The Ca_V pore-forming $Ca_V\alpha_1$ subunit is a 24 transmembrane segment protein comprising four repeats (DI–DIV) that are each made from six transmembrane helices that form the voltage sensor domain (SI–S4) and the pore domain (S5–S6) (Catterall et al., 2017; Wu et al., 2015, 2016). $Ca_V\alpha_1$ shares the overall architecture found throughout the voltage-gated ion channel (VGIC) superfamily but requires auxiliary subunits for proper function (Campiglio and Flucher, 2015; Dolphin, 2016). Complexes with two intracellular components that bind to the cytosolic I-II loop and C-terminal tail, the $Ca_V\beta$ subunit (Chen et al., 2004; Opatowsky et al., 2004; Van Petegem et al., 2004) and calmodulin (CaM) (Fallon et al., 2009; Kim et al., 2008, 2010; Mori et al., 2008; Van Petegem et al., 2005), respectively, are particularly important for activity-dependent feedback modulation by the two principal Ca_V inactivation mechanisms, voltage-dependent inactivation (VDI) (Cens et al., 2006; Stotz et al., 2004) and CDI (Ben-Johny and Yue, 2014; Cens et al., 2006; Christel and Lee, 2011; Halling et al., 2006).

The molecular origins of CDI have been extensively investigated, especially from the vantage point of the intracellular, CaM-based sensor apparatus and the role of the CaM-binding IQ domain (Ben-Johny and Yue, 2014; Fallon et al., 2005; Minor and Findeisen, 2010; Kim et al., 2008, 2010; Mori et al., 2008; Van Petegem et al., 2005). Although the involvement of this CaM-based sensor in CDI is clear (Ben-Johny and Yue, 2014; Minor and Findeisen, 2010; Kim et al., 2008, 2010; Lee et al., 1999; Mori et al., 2008; Peterson et al., 1999; Van Petegem et al., 2005; Zühlke et al., 1999), the fact that the N-terminal cytoplasmic domain (Ben Johny et al., 2013; Dick et al., 2008; Ivanina

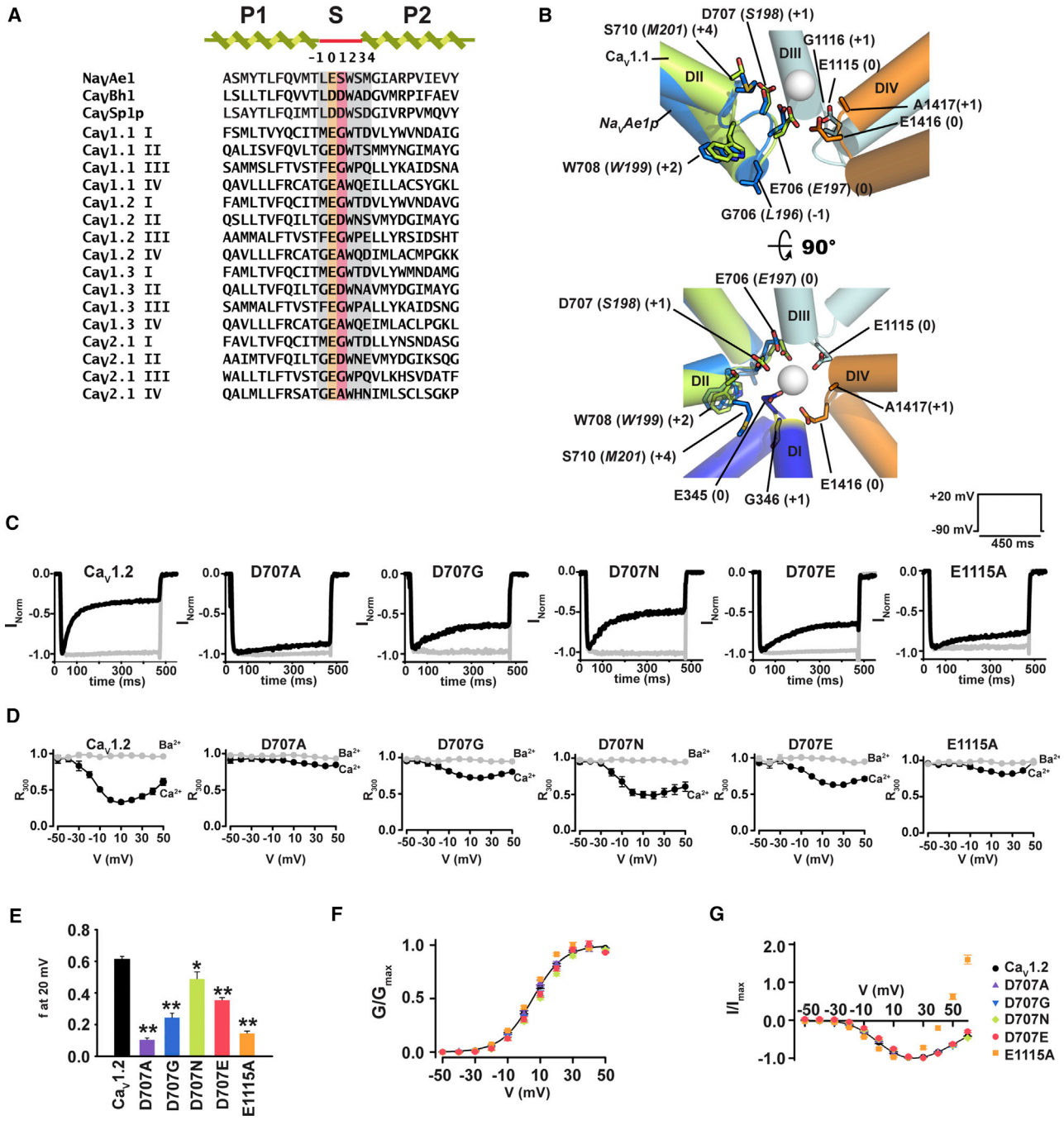

Figure 1. $Ca_V1.2$ Selectivity Filter Mutations in DII Affect CDI

(A) Sequence alignment of pore helices and selectivity filters of Na_VAe1 (Shaya et al., 2014), calcium-selective BacNa$_V$s Ca_VBh1 (Yue et al., 2002), Ca_VSp1p (Shaya et al., 2011), and human Ca_V1 and Ca_V2 exemplars: $Ca_V1.1$ (UniProtKB: Q13698), $Ca_V1.2$ (UniProtKB: Q13936), $Ca_V1.3$ (UniProtKB: Q01668), and $Ca_V2.1$ (UniProtKB: O00555). SF sites (0) and (+1) are highlighted in orange and red, respectively. Other SF sites are highlighted in gray. Sequences are Na_VAe1 185-211, Ca_VBh1 179-205, Ca_VSp1p 164-190, $Ca_V1.1$ DI 280-306, $Ca_V1.1$ DII 602-628, $Ca_V1.1$ DIII 1002-1028, $Ca_V1.1$ DIV 1311-1337, $Ca_V1.2$ DI 351-377, $Ca_V1.2$-DII 694-720; $Ca_V1.2$-DIII 1103-1129, $Ca_V1.2$-DIV 1404-1430, $Ca_V1.3$-DI: 343-369, $Ca_V1.3$-DII 704-730, $Ca_V1.3$ DIII 1100-1126, $Ca_V1.3$ DIV 1390-1416, $Ca_V2.1$-DI 306-332, $Ca_V2.1$ DII 656-682, $Ca_V2.1$ DIII 1448-1474, $Ca_V2.1$ DIV 1744-1770.

(B) Structural comparison of the Na_VAe1 (PDB: 5HK7) (Arrigoni et al., 2016) SF (marine) with the $Ca_V1.1$ (PDB: 5GJV) (Wu et al., 2016) DII SF (green). Ca^{2+} from Na_VAe1 (PDB: 4LTO) (Shaya et al., 2014) is shown as a sphere. DI (blue), DII (green), DIII (cyan), and DIV (orange) domains of $Ca_V1.1$ are shown. $Ca_V1.1$ and Na_VAe1p residues are labeled in plain and italics, respectively. Ca_V numbering follows the $Ca_V1.2$ equivalent residues. SF positions are shown in parentheses. Side view (top) omits DI for clarity. DI (+1) position is highlighted in yellow.

(C) Exemplar normalized recordings at +20 mV in Ca^{2+} (black) or Ba^{2+} (gray) from *Xenopus* oocytes expressing $Ca_V1.2$ or indicated mutants.

(legend continued on next page)

et al., 2000; Tadross et al., 2008) and the $Ca_V\beta$/I-II loop complex (Almagor et al., 2012; Findeisen and Minor, 2009) also impact CDI has left open the question of how conformational changes in these cytoplasmic parts of the channel complex terminate Ca^{2+} influx (Babich et al., 2007; Barrett and Tsien, 2008; Cens et al., 2006; Findeisen and Minor, 2009; Kim et al., 2004; Tadross et al., 2010). The prevailing model suggests that the activation gate formed by the S6 helices of the channel pore acts as the CDI endpoint via an allosteric mechanism (Dick et al., 2016; Limpitikul et al., 2016; Tadross et al., 2010). Other studies have raised the idea of a close link between ion selectivity and CDI, based on the fact that CDI and selectivity properties are simultaneously affected by SF mutations or changes in extracellular Ca^{2+} concentrations (Babich et al., 2005; Zong et al., 1994) and on the observation that SF Gd^{3+} block appears mutually exclusive with inactivation (Babich et al., 2007). Further, the extent to which CDI and VDI share common pathways (Cens et al., 1999; Findeisen and Minor, 2009; Kim et al., 2004) or act by different mechanisms (Barrett and Tsien, 2008; Tadross et al., 2010) has been unclear.

We discovered that mutations in the conserved aspartate at the $Ca_V1.2$ domain II (DII) SF (+1) position, a site that is important for Ca_V SF Ca^{2+} binding and that forms an outer ion binding site in bacterial voltage-gated sodium channels ($BacNa_Vs$) and mammalian Ca_Vs (Shaya et al., 2014), affect CDI. Mutation of this conserved aspartate can effectively eliminate CDI in $Ca_V1.2$, while sparing core biophysical properties including voltage-dependent activation, VDI, and ion selectivity. Analogous SF DII (+1) mutations in two other Ca_Vs, a $Ca_V1.3$ variant bearing the most robust CDI among all Ca_Vs (Huang et al., 2013; Singh et al., 2008; Xu and Lipscombe, 2001) and $Ca_V2.1$, a channel in which CDI relies on a different CaM lobe than in Ca_V1 s (DeMaria et al., 2001; Minor and Findeisen, 2010; Lee et al., 2003; Liang et al., 2003), demonstrate that the role of the DII (+1) aspartate in controlling CDI is both conserved and independent of the details of how the intracellular Ca^{2+} sensor acts. We also show that, in channels lacking CDI because the DII (+1) aspartate is mutated, one can restore CDI by placing an aspartate at the analogous SF (+1) sites of DIII or DIV but not DI. This observation is concordant with asymmetric functional roles for the four glutamates at the SF (0) position (Ellinor et al., 1995; Parent and Gopalakrishnan, 1995; Yang et al., 1993) and indicates that the change in the SF that drives CDI is asymmetric. Together, our data establish that the Ca_V SF is the endpoint gate for CDI and change the paradigm for understanding Ca_V inactivation mechanisms by placing it squarely within the framework of the growing list of VGIC superfamily members in which SF-based gating is central to function (Autzen et al., 2018; Bagriantsev et al., 2011; Cao et al., 2013; Cohen et al., 2008; Cuello et al., 2010, 2017; Liu et al., 1996; Lolicato et al., 2017; López-Barneo et al., 1993; Ogielska and Aldrich, 1999; Pavlov et al., 2005; Peters et al., 2013; Piechotta et al., 2011; Schewe et al., 2016; Steinberg et al., 2017). These findings support the idea that SF inactivation is an ancient process arising from the conserved VGIC pore architecture (Catterall et al., 2017) that not only affects slow inactivation, but also controls CDI in Ca_Vs.

RESULTS

Single $Ca_V1.2$ Selectivity Filter Mutations Drastically Reduce CDI in *Xenopus* Oocytes

The SF sequences of each of the four Ca_V domains are highly similar to each other and to those found in $BacNa_Vs$ (Payandeh and Minor, 2015; Ren et al., 2001; Shaya et al., 2014; Wu et al., 2015; Yue et al., 2002), which are thought to be a common ancestor of both voltage-gated sodium channels (Na_Vs) and Ca_Vs (Koishi et al., 2004; Payandeh and Minor, 2015; Ren et al., 2001). All share the central glutamate residue (denoted position (0); Payandeh and Minor, 2015; Shaya et al., 2014) (Figure 1A) and a common architecture that supports the SF structure (Figure 1B) (Payandeh and Minor, 2015; Payandeh et al., 2011; Wu et al., 2015). The SF (0) position glutamates form a charged ring at the center of the Ca_V and $BacNa_V$ SFs (Payandeh and Minor, 2015; Payandeh et al., 2011; Wu et al., 2015, 2016) and play a key role in Ca^{2+} selectivity and ion permeation (Parent and Gopalakrishnan, 1995; Yang et al., 1993). In the case of Ca_Vs, the four SF sequences are not identical. Further, even though the side-chain identity at the Ca_V SF position (0) is the same, each (0) position glutamate contributes differently to SF properties with the DIII (0) glutamate ($Ca_V1.2$ Glu 1115) being the most important contributor to ion selectivity (Ellinor et al., 1995; Kim et al., 1993; Mikala et al., 1993; Yang et al., 1993). A further asymmetry in the Ca_V SF occurs at DII position (+1). This site has a unique aspartate ($Ca_V1.2$ Asp 707) (Figure 1A) that is involved in the high-affinity binding of Ca^{2+} to the SF and whose neutralization by mutation has similar effects on Ca^{2+} binding as neutralization of the DIII position (0) glutamate (Shaya et al., 2014).

In the course of studying the functional properties of $Ca_V1.2$ SF mutants using two-electrode-voltage clamp of *Xenopus* oocytes (Figure S1A), we observed that replacement of the DII (+1) site, Asp 707, with alanine, glycine, asparagine, or glutamate decreased CDI. These effects manifested as varied degrees of reduction of the classic "U-shaped" response characteristic of CDI with D707A and D707N causing the greatest and mildest effects, respectively (Figures 1C and 1D).

To quantify changes in CDI, we measured the ratio between the current amplitude at the peak and 300 ms post-depolarization (R_{300}) for both Ba^{2+} and Ca^{2+} as a function of voltage (Figure 1D) and compared the difference between Ba^{2+} and Ca^{2+} R_{300} values, f, for $Ca_V1.2$ and D707A/G/N/E mutants at the potential of maximal current, +20 mV (Peterson et al., 1999). This

(D) Fractional current remaining 300 ms post-depolarization (R_{300}) as a function of the membrane potential for channels in (C).

(E) Average fraction CDI (f) at +20 mV, where f is the difference between Ca^{2+} and Ba^{2+} R_{300}. *$p < 0.015$ and **$p < 0.001$ compared to $Ca_V1.2$. n values are in Table 1.

(F) Voltage-dependent activation curves for $Ca_V1.2$ (black circles), D707A (purple triangles), D707G (inverted blue triangles), D707N (green diamonds), D707E (red circles), and E1115A (orange squares).

(G) I–V relationships for the indicated channels. Symbols are the same as (F).

Table 1. Electrophysiological Parameters

	Channel	f or f′	I_{Ba}/I_{Ca}	E_{rev}	$V_{1/2}$	k	n
Oocytes	$Ca_V1.2$	0.61 ± 0.02	1.72 ± 0.11	89.1 ± 4.0	5.4 ± 0.6	9.5 ± 0.3	8
	D707A	0.10 ± 0.01	1.53 ± 0.05	92.8 ± 4.8	5.2 ± 0.9	9.8 ± 0.5	13
	D707G	0.24 ± 0.03	1.94 ± 0.13	94.8 ± 4.0	7.2 ± 0.8	9.0 ± 0.6	5
	D707N	0.49 ± 0.04	2.63 ± 0.03	87.8 ± 2.5	10.0 ± 0.6	9.8 ± 0.5	5
	D707E	0.35 ± 0.02	3.58 ± 0.24	88.0 ± 8.1	8.5 ± 1.0	8.7 ± 0.5	6
	E1115A	0.14 ± 0.02	0.92 ± 0.01	49.8 ± 1.0	1.7 ± 0.3	8.6 ± 0.2	8
	G364D-D707G	0.30 ± 0.02	2.98 ± 0.26	88.7 ± 6.1	10.4 ± 1.2	9.3 ± 0.2	7
	D707G-G1116D	0.60 ± 0.02	2.28 ± 0.29	89.2 ± 4.3	4.8 ± 3.3	8.1 ± 0.6	6
	D707A-A1417D	0.45 ± 0.01	1.63 ± 0.14	83.9 ± 4.2	5.2 ± 1.1	8.9 ± 0.4	9
	E1119A	0.59 ± 0.02	1.73 ± 0.18	88.9 ± 3.6	6.3 ± 1.1	9.1 ± 0.2	6
	D1420A	0.60 ± 0.02	1.88 ± 0.23	79.3 ± 2.7	5.8 ± 1.9	10.0 ± 0.2	5
HEK293	Ca_V 1.2	0.59 ± 0.02	1.57 ± 0.38	77.5 ± 3.0	7.1 ± 2.0	6.5 ± 0.6	8
	D707A	0.17 ± 0.02	1.94 ± 0.21	80.5 ± 1.8	11.8 ± 0.5	8.7 ± 0.2	6
	D707E	0.40 ± 0.04	2.86 ± 0.52	73.3 ± 2.9	11.3 ± 2.1	6.8 ± 0.5	4
	E1115A	0.36 ± 0.04	1.00 ± 0.15	68.5 ± 1.5	−0.5 ± 2.0	7.8 ± 0.5	6
	$Ca_V1.3$	0.73 ± 0.01	1.58 ± 0.11	75.6 ± 3.0	−8.5 ± 1.1	7.3 ± 0.5	6
	D726A	0.15 ± 0.05	1.85 ± 0.16	81.1 ± 1.3	−8.6 ± 0.9	7.1 ± 0.4	8
	E1121A	0.63 ± 0.02	1.09 ± 0.08	61.9 ± 3.0	−15.3 ± 1.7	7.8 ± 0.4	9
	$Ca_V2.1$	0.26 ± 0.03	1.64 ± 0.39	46.9 ± 7.0	−7.7 ± 0.8	3.2 ± 0.6	7
	D667A	0.04 ± 0.03	1.81 ± 0.12	56.4 ± 3.2	−4.7 ± 1.4	3.8 ± 0.9	6
	E1461A	0.12 ± 0.02	1.07 ± 0.13	34.0 ± 1.2	−8.8 ± 0.5	3.4 ± 0.2	5

f is defined as R_{300} for Ba^{2+} – R_{300} for Ca^{2+} where $R_{300} = I_{300}/I_0$ where I_{300} and I_0 are current amplitudes at 300 ms post-depolarization and at the peak current, respectively. f′ is defined as R_{800} for Ba^{2+} – R_{800} for Ca^{2+} where $R_{800} = I_{800}/I_0$ where I_{800} and I_0 are current amplitudes at 800 ms post-depolarization and at the peak current, respectively. f and f′ were determined at membrane potential of +20 and +10 mV, respectively. I_{Ba}/I_{Ca} is the Ba^{2+} and Ca^{2+} peak current amplitude ratio. E_{rev} is the reversal potential. $V_{1/2}$ is the midpoint of activation. k is the slope factor of the activation curve. E_{rev}, $V_{1/2}$, and k were determined using Ca^{2+} as the charge carrier. n is the number of experiments. Data were fit to $I = G_{max} * (V_m - E_{rev})/(1 + \exp(V_{1/2} - V_m)/k)$, where I is the measured peak current at each test potential (V_m) and G_{max} is the maximal macroscopic conductance. Data are expressed as mean values ± SEM.

analysis revealed a rank order of D > N > E > G > A (f = 0.61 ± 0.02, 0.49 ± 0.04, 0.35 ± 0.02, 0.24 ± 0.03, and 0.10 ± 0.01, respectively; Table 1), suggesting the importance of both the negative charge and the DII (+1) position side-chain geometry for CDI. The stronger CDI observed in D707N versus D707E indicates that other side-chain properties at the DII (+1) besides the negative charge are important for CDI. Experiments using a domain III position (0) mutant that reduces Ca^{2+} ion selectivity, E1115A (Ellinor et al., 1995; Mikala et al., 1993), also caused a large reduction in CDI (f = 0.14 ± 0.02) that was comparable to the Asp 707 mutant causing the most severe CDI reduction, D707A (Figures 1C–1E). None of the SF mutants that we tested affected voltage-dependent activation (Figure 1F). Consistent with its ability to reduce Ca^{2+} selectivity (Ellinor et al., 1995; Mikala et al., 1993), the E1115A mutant caused a shift in the reversal potential for Ca^{2+} relative to wild-type (E_{rev} = 89.1 ± 4.0 mV and 49.8 ± 1.0 mV for $Ca_V1.2$ and E1115A, respectively) (Figure 1G). Such a change in E_{rev} was notably absent from the Asp 707 mutants, all of which behaved similarly to wild-type (E_{rev} = 92.8 ± 4.8, 94.8 ± 4.0, 87.8 ± 2.5, and 88.0 ± 8.1 mV for D707A, D707G, D707N, and D707E, respectively) (Figure 1G). E1115A reduced the ratio between Ba^{2+} and Ca^{2+} peak currents (I_{Ba}/I_{Ca}) to a value close to one, indicating that this mutation renders the SF unable to discriminate between Ba^{2+} and Ca^{2+}, and consistent with a change in ion selectivity. By contrast, the ability to discriminate between Ba^{2+} and Ca^{2+} was preserved in all Asp 707 mutants, as I_{Ba}/I_{Ca} was either unaffected (D707A, D707G) or increased (D707N, D707E) (Figure S2A). Moreover, switching the $Ca_V\beta$ subunit to $Ca_V\beta_3$, a subunit that allows fast VDI (De Waard and Campbell, 1995; Stea et al., 1994) did not alter the relative impact of the Asp 707 mutations on CDI, a result demonstrating that SF mutation effects on CDI are independent of $Ca_V\beta$ (Figure S3). Overall, these observations indicate that Asp 707 mutations affect CDI but leave other biophysical properties unchanged.

SF Mutations Identify Elements that Selectively Affect CDI or VDI

Ca_Vs have two principal inactivation mechanisms, CDI (Ben-Johny and Yue, 2014; Cens et al., 2006; Halling et al., 2006) and VDI (Cens et al., 2006; Stotz et al., 2004). Due to the strong slowing effects that $Ca_V\beta_{2a}$ has on VDI (De Waard and Campbell, 1995; Olcese et al., 1994; Stea et al., 1994), VDI is largely absent in our initial experiments that uncovered the importance of the DII (+1) site in CDI (Figures 1C and 1D). Therefore, to examine the possible impact of changes at the DII (+1) SF position on VDI, we paired $Ca_V1.2$ channels bearing a set of DII (+1) mutations that had differing effects on CDI (D707A, D707E, and

D707N) with the $Ca_V\beta$ isoform that imparts the fastest VDI, $Ca_V\beta_3$ (De Waard and Campbell, 1995; Stea et al., 1994), and measured the effects on VDI kinetics using Ba^{2+} as the charge carrier. These experiments showed that regardless of whether the DII (+1) SF mutant caused a strong (D707A), intermediate (D707E), or mild (D707N) effect on CDI, none caused changes in VDI (Figures 1C, 1D, S4A, and S4B).

Mutations at the SF (+4) site on the extracellular side of the pore above the SF (+1) and (0) positions (Figure 1B) affect inactivation in $BacNa_Vs$ (Pavlov et al., 2005), bacterial channels sharing both structural and functional properties with Ca_Vs and Na_Vs (Catterall et al., 2017; Payandeh and Minor, 2015). To ask whether mutations at the three homologous $Ca_V1.2$ SF (+4) positions bearing charged residues, DI Asp 367, DIII Glu 1119, and DIV Asp 1420 (Figure 1A), could affect Ca_V inactivation, we measured the effect of alanine mutations at each of these sites in $Ca_V1.2$ co-expressed with $Ca_V\beta_3$. Two of the three mutations, DIII (+4) E1119A and DIV (+4) D1420A, reduced both the rate and the extent of VDI. By contrast, DI (+4) D367A had no effect on VDI (Figures S4C and S4D). Interestingly, despite the clear effects of DIII (+4) E1119A and DIV (+4) D1420A on VDI, these mutations left CDI and other biophysical properties completely intact (Figure S5). These experiments demonstrate that removal of the conserved negative charges at two different levels of the SF architecture yields two distinct phenotypic outcomes. Removal of the negative charge at DII (+1) blunts CDI but spares VDI, whereas removal of the negative charge at DIII (+4) or DIV (+4) leaves CDI intact but reduces VDI. These results support the general idea that inactivation mechanisms are set by the shared nature of the pore domain architecture across diverse VGICs (Catterall et al., 2017). The ability of the DII (+1) mutants to blunt CDI but spare VDI and other biophysical properties differs from the consequences of cytoplasmic domain mutations that affect CDI but that also impact coupling to the $Ca_V\beta$ subunit and VDI (Findeisen and Minor, 2009), and S6 mutations that affect CDI but that also affect VDI and activation voltage dependency (Limpitikul et al., 2016; Tadross et al., 2010). Together, our observations suggest that the SF is an essential element in the CDI mechanism.

Single $Ca_V1.2$ SF Mutations Drastically Reduce CDI in Mammalian Cells

Our observations suggest two possible mechanisms by which the DII (+1) and DIII (0) SF mutants could diminish CDI. The first, consistent with the effects of the DIII (0) mutant E1115A, is that mutations at some SF sites cause ion selectivity changes that reduce Ca^{2+} ion influx and, thereby, reduce CDI. The second, suggested by the DII (+1) position Asp 707 mutations, is that key portions of the SF play an active role in CDI. Because the loss of the negatively charged residue at DII (+1) did not dramatically alter channel selectivity properties or activation voltage dependency, we pursued further characterization of this site to understand whether the Ca_V SF might have a previously unappreciated role in the CDI mechanism.

Alteration of the CaM binding IQ motif has different impacts on $Ca_V1.2$ CDI depending on whether oocytes or mammalian cells are used to measure function (Barrett and Tsien, 2008). Therefore, to test whether the consequences of SF mutations on CDI were similarly expression system dependent, we measured the properties of the two mutants that had the strongest effects on CDI reduction of $Ca_V1.2$ in oocytes, D707A and E1115A, as well as the mutant that maintained the SF DII (+1) negative charge, D707E, using whole-cell recordings from transfected HEK293 cells (Figures 2A and S1B). As in oocytes, D707A, D707E, and E1115A caused a substantial reduction in CDI (Figures 2A–2C). The magnitude of the CDI diminishment was less pronounced in the E1115A mutant compared to oocytes, whereas this effect was comparable between the two different expression systems for D707A and D707E (Table 1). Similar to oocytes, voltage-dependent activation and I-V curves of $Ca_V1.2$ and Asp 707 mutants were identical (Figures 2D and 2E). E1115A caused a small hyperpolarizing shift (−8 mV) in voltage-dependent activation, not seen in oocytes (Figure 2E; Table 1), and perturbed the reversal potential, although this change is smaller in HEK293 cells (−9 versus −39 mV for HEK293 cells and *Xenopus* oocytes, respectively) (Figures 1G and 2E; Table 1). In further support of differential effects of the mutants on ion selectivity, similar to oocytes, the ability to discriminate Ca^{2+} over Ba^{2+}, reflected by $I_{Ba}/I_{Ca} > 1$, was conserved in the Asp 707 mutants but was eliminated in E1115A (Figure S2B; Table 1). Thus, in contrast to expression system-dependent differences in CDI at the level of the Ca^{2+} sensor (Barrett and Tsien, 2008), our results demonstrate that the SF mutation-induced CDI changes are expression system independent and provide additional support for the idea that the reduction in CDI caused by the DII (+1) mutants are not related to changes in the ion selectivity properties of the channel.

Lowered Ca^{2+} Influx in DII (+1) Mutants Does Not Cause Loss of CDI

Although the DII (+1) mutations did not cause ion selectivity changes, in principle, the effects on CDI could be caused by reduction of Ca^{2+} influx via a change in channel open probability or conductance. To investigate this possibility, we compared low-noise recordings from the DII (+1) mutants that exhibited the most severe, D707A, and the mildest, D707N, CDI loss with $Ca_V1.2$. Because of the challenges associated with single Ca_V channel recordings when Ca^{2+} is the charge carrier (Hess et al., 1984), we compared patches expressing $Ca_V1.2$, D707A, and D707N using Ba^{2+} as the charge carrier as in many prior studies (Adams et al., 2014; Bock et al., 2011; Dick et al., 2016; Doering et al., 2005; Hess et al., 1984; Tadross et al., 2008, 2013; Yang et al., 2015). These experiments showed single $Ca_V1.2$ channels having an ~1-pA current amplitude, consistent with prior reports (Dick et al., 2016). By contrast, in patches expressing either D707A or D707N, we could only observe measurable currents characteristic of multi-channel recordings with maximal current of ~2 pA (Figure 3A). These observations indicate that both the D707A and D707N decrease channel conductance relative to wild-type. To address whether there was a parallel reduction in Ca^{2+} conductance relative to the reduced level of CDI, we measured whole-cell Ca^{2+} currents of $Ca_V1.2$, D707A, and D707N (Figure 3B) and compared their current densities (Figure 3C). These data reveal similar current densities for D707A and D707N that are both reduced by ~80% relative to $Ca_V1.2$ (Figure 3C) and that are consistent with the reduced

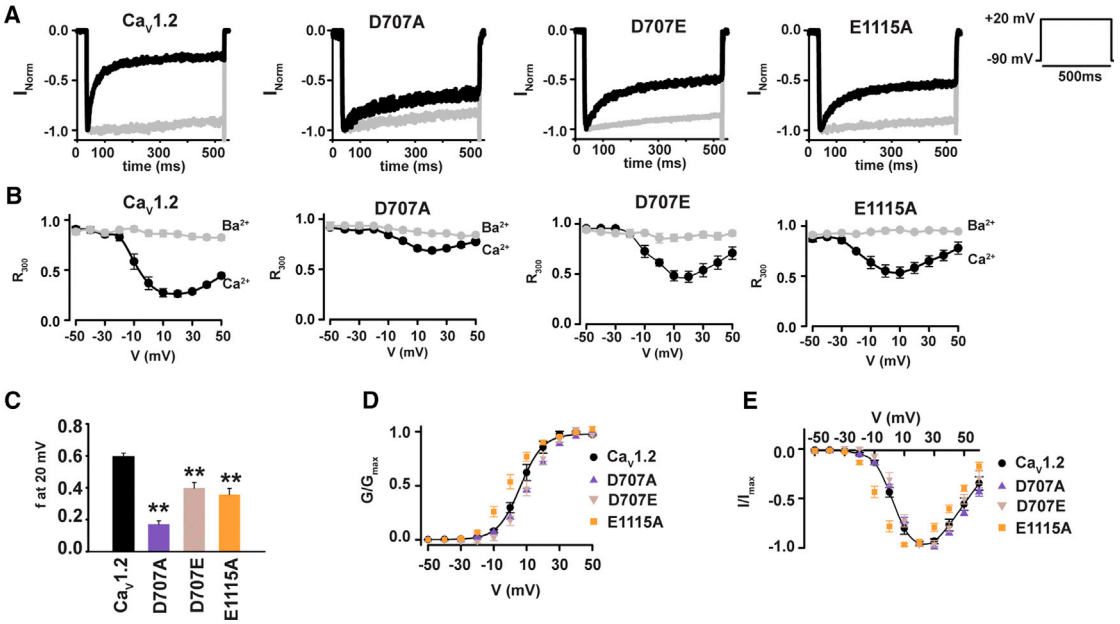

Figure 2. Domain II SF Mutations Reduce CDI in Ca$_V$1.2 Expressed in Mammalian Cells

(A) Exemplar normalized recordings at +20 mV in Ca^{2+} (black) or Ba^{2+} (gray) from HEK293 cells expressing Ca$_V$1.2 or the indicated mutants.

(B) Fractional current remaining 300 ms post-depolarization (R_{300}) as a function of the membrane potential for channels in (A).

(C) Average f values at 20 mV. **$p < 0.001$ compared to Ca$_V$1.2.

(D) Voltage-dependent activation curves for Ca$_V$1.2 (black circles), Ca$_V$1.2 D707A (purple triangles), Ca$_V$1.2 D707E (tan inverted triangles), and Ca$_V$1.2 E1115A (orange squares). Currents are normalized to the maximum peak current.

(E) I–V relationships for the indicated channels. Symbols are as in (D).

channel conductance assessed by the low-noise recordings (Figure 3A). The reduced single-channel conductance observed for D707A and D707N is in line with the ability of both mutants to cause similar reductions in Ca^{2+} binding to the channel pore (Shaya et al., 2014) and points to a key role of the DII (+1) site in ion conduction. Importantly, the data indicate that the shared decrease in ion conduction caused by the DII (+1) mutations cannot be the origin of the loss of CDI in D707A, as two channels having similar low conductances, D707A and D707N, have completely different CDI phenotypes (Figures 1C–1E).

To investigate whether reduced Ca^{2+} influx was the cause of CDI loss in D707A, we used the Ca$_V$ agonist Bay K8644 that increases single-channel open times (Hess et al., 1984) to enhance Ca^{2+} influx through the channel. Bay K8644 application to *Xenopus oocytes* expressing Ca$_V$1.2, D707A, D707N, or the mutant E1115A, in which changes in ion selectivity reduce Ca^{2+} influx (Ellinor et al., 1995; Mikala et al., 1993), showed clear augmentation in Ca^{2+} current amplitude for all cases, consistent with an increase in channel openings and higher Ca^{2+} influx through individual channels (Hess et al., 1984) (Figures 3D and 3F). This Bay K8644-enhanced Ca^{2+} current was accompanied by a more complete inactivation for Ca$_V$1.2, D707N, and E1115A as measured by the percentage of inactivation 300 ms post-activation (t_{i300}) (Figures 3D and 3G), consistent with prior studies of Bay K8644 on Ca$_V$1.2 in *Xenopus* oocytes (Noceti et al., 1998). However, for Ca$_V$1.2 and D707N, the equivalent level of increased inactivation was also observed when Ba^{2+} was used as charge carrier, indicating that this effect is a consequence of Bay K8644 itself rather than a response to the increased Ca^{2+} influx due to an undersaturated CaM Ca^{2+} sensor (Figures 3D, 3H, and 3I). By contrast, for the mutant having compromised selectivity, E1115A, CDI was enhanced beyond the level expected from the Bay K8644 effect in Ba^{2+} (Figure 3I). Notably, Bay K8644-induced inactivation in Ca^{2+} is absent in the D707A mutant (Figures 3D, 3E, and 3G–3I). Hence, even though the magnitude of the Bay K8644-induced Ca^{2+} current increase was similar for Ca$_V$1.2, D707A, and D707N (Figure 3F), the enhanced Ca^{2+}-influx was not able to induce CDI for D707A (Figures 3E and 3G). Taken together, these observations establish that CDI loss in the D707A mutant is not caused by a reduced Ca^{2+} influx and strongly suggest that SF DII (+1) position plays an active role in CDI.

A Single Ca$_V$1.3 SF DII (+1) Mutation Drastically Reduces CDI

The aspartate at the SF DII (+1) site is conserved among all Ca$_V$s (Figure 1A) (Payandeh and Minor, 2015; Shaya et al., 2014). CDI occurs in high voltage-activated Ca$_V$s (Ca$_V$1s and Ca$_V$2s) (Liang et al., 2003), and, among the L-type (Ca$_V$1) channels, the Ca$_V$1.3$_{42a}$ variant exhibits the most pronounced CDI (Huang et al., 2013; Singh et al., 2008; Xu and Lipscombe, 2001). Therefore, to examine the general importance of the DII (+1) aspartate for CDI, we asked whether removal of this aspartate would affect a channel in which CDI is particularly strong. We compared Ca$_V$1.3$_{42a}$ CDI with a DII (+1) mutant and a DIII (0) mutant (D762A and E1121A, respectively) that correspond to the

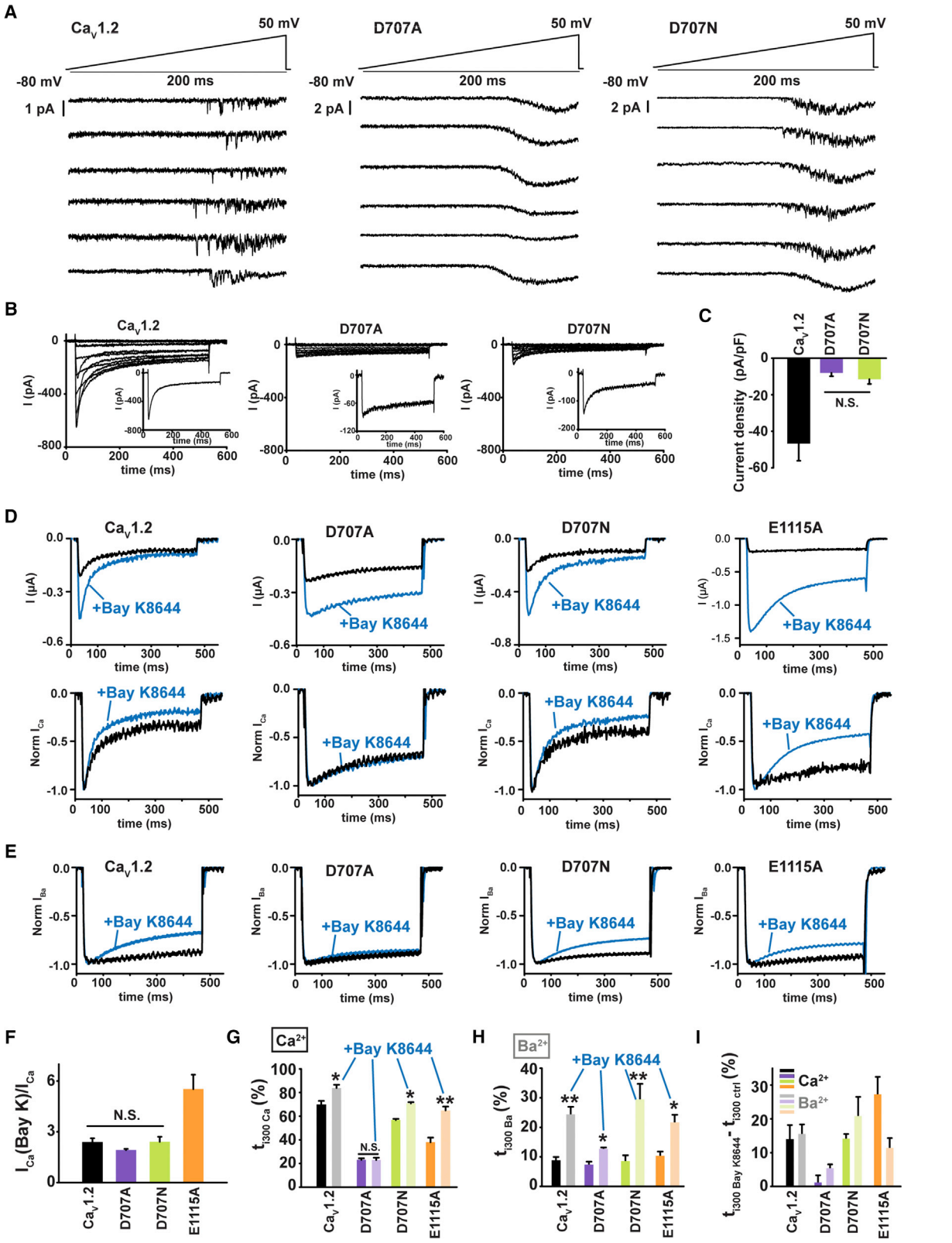

(legend on next page)

mutants that were most effective at reducing $Ca_V1.2$ CDI. Measurement of the functional properties of these channels in HEK293 cells showed that, as with the analogous $Ca_V1.2$ mutants, the DII (+1) mutation D726A drastically reduced CDI, whereas the DIII (0) mutation E1121A caused only a slight reduction in CDI (f = 0.73 ± 0.01, 0.15 ± 0.05, and 0.63 ± 0.02 for $Ca_V1.3$, D726A, and E1121A, respectively; Figures 4A–4C; Table 1). Similar to our observations for $Ca_V1.2$, the DII (+1) mutant D726A had no effect on channel selectivity or the activation voltage dependency (Figures 2D and 2E; Table 1), whereas the DIII (0) mutant, E1121A, caused a slight leftward shift of both the reversal potential and the activation curve, comparable to the effects of E1115A on $Ca_V1.2$ (Figures 2D, 2E, 4D, and 4E; Table 1). In addition, unlike the DII (+1) D726A change, the DIII (0) E1121A substitution caused a significant reduction in the peak current I_{Ba}/I_{Ca} ratio to ~1, indicating a loss in the ability to discriminate between Ba^{2+} and Ca^{2+} (Figure S2C; Table 1). Hence, as with $Ca_V1.2$, the effects of neutralizing the DIII (0) glutamate with respect to the observed CDI reduction are consistent with a change in ion selectivity. By contrast, neutralization of the DII (+1) aspartate spared all of the tested $Ca_V1.3$ biophysical parameters, except CDI. These results demonstrate the general importance of the DII (+1) aspartate in Ca_V1 channels and lend further support to the hypothesis that changes in the SF have a direct role in CDI.

SF DII (+1) Aspartate Is Generally Important for CDI

Ca_V2 channels also have CDI (DeMaria et al., 2001; Lee et al., 2003; Liang et al., 2003), and, similar to Ca_V1s, this process relies on CaM:IQ domain interactions (Ben-Johny and Yue, 2014; Dunlap, 2007; Minor and Findeisen, 2010). However, the roles of the CaM lobes are inverted between the two subfamilies, with the C-lobe controlling CDI in Ca_V1 (Peterson et al., 1999) but the N-lobe controlling CDI in Ca_V2s (DeMaria et al., 2001; Lee et al., 2003; Liang et al., 2003). To ask whether the conserved DII (+1) aspartate is important for Ca_V CDI regardless of which CaM lobe governs CDI, we measured the effects of mutants equivalent to $Ca_V1.2$ DII (+1) D707A and DIII (0) E1115A in a Ca_V2 family representative, $Ca_V2.1$ (D667A and E1461A, respectively). To quantify changes in $Ca_V2.1$ CDI, we measured the ratio between the current amplitude at peak and 800 ms post-depolarization (R_{800}) for both Ba^{2+} and Ca^{2+} as a function of voltage (DeMaria et al., 2001) (Figures 4F and 4G) and compared the difference between Ba^{2+} and Ca^{2+} R_{800}, f′, for $Ca_V2.1$ and mutants at the potential of maximal current, +10 mV (DeMaria et al., 2001). As in the case of $Ca_V1.2$ and $Ca_V1.3$, DIII (0) neutralization caused a CDI reduction (f′ = 0.26 ± 0.03 and 0.12 ± 0.02 for $Ca_V2.1$ and E1461A, respectively; Figure 4H) and did not affect activation voltage dependency. However, this site (0) mutation did induce a −13 mV reversal potential shift and reduced peak current I_{Ba}/I_{Ca} ratio to ~1 (Figures 4H–4J and S2D; Table 1), consistent with an ion selectivity change. By contrast, neutralization of the $Ca_V2.1$ DII (+1) residue essentially eliminated CDI (f′ = 0.04 ± 0.03; Figure 4H) and did not affect the activation voltage dependency or the peak current I_{Ba}/I_{Ca} ratio (Figures 4J and S2D; Table 1), although it did cause a +10 mV reversal potential shift (Figure 4I). The clear loss of $Ca_V2.1$ CDI caused by the D667A mutation demonstrates the universal role of the Ca_V SF in CDI and establishes that this role is independent of the details of how the CDI is initiated by CaM. Together with the Ca_V1 results, these data support the idea that the SF is involved in the final step of the Ca_V CDI process.

CDI Requires a Negative Charge at SF (+1) Position on DII, DIII, or DIV

The four Ca_V SF domains contribute an identical set of negatively charged glutamate side chains at the (0) position but a set of non-equivalent residues at the (+1) site (G, D, G, and A for DI–DIV, respectively) (Figures 1A and 1B). Given the crucial role we found for the DII (+1) aspartate in CDI (Figures 5A and 5B), and the fact that it is the sole negatively charged amino acid at this Ca_V SF level, we asked whether the DII (+1) position had a special role in CDI or whether CDI would be preserved if the aspartate were moved to other (+1) positions around the SF. Hence, we created a set of mutants that placed an aspartate at the DI, DIII, or DIV (+1) sites. To preserve the SF amino acid composition, each of these mutants exchanged the amino acid from the host site into the DII (+1) site to create the following swap mutants: DI_{Asp} (G364D/D707G), $DIII_{Asp}$ (D707G/G1116D), and DIV_{Asp} (D707A/A1417D) (Figure 5C). We recorded whole-cell currents from *Xenopus* oocytes injected with these constructs using Ca^{2+} and Ba^{2+} as charge carriers and compared these mutants with the corresponding single-point changes at DII (+1) (Figures 5C and 5D). Exchange of the SF (+1) aspartate between the DII and DI positions, DI_{Asp}, yielded channels that had severely diminished CDI that was equivalent to the D707G

Figure 3. CDI Loss in the SF (+1) Mutant D707A Is Unrelated to Insufficient Ca^{2+} Influx

(A) Exemplar cell-attached low noise current recordings in response to a voltage ramp (top) for HEK293 cells expressing $Ca_V1.2$ or the indicated mutants. Each trace is from a different patch.

(B) Exemplar whole-cell current recordings from HEK293 cells expressing $Ca_V1.2$ or the indicated mutants. Currents were evoked with a multistep depolarization protocol from −50 to +50 mV using 10 mV increments and a −90 mV holding potential. Exemplar current traces at +20 mV are shown (inset).

(C) Current densities for $Ca_V1.2$ and the indicated mutants. N.S., not statistically different; n = 6–7.

(D) Exemplar Ca^{2+} currents from *Xenopus* oocytes expressing $Ca_V1.2$ or the indicated mutants, in response to a +20 mV depolarization in absence (black) or in presence of 5 μM Bay K8644 (blue). Raw traces (upper panel) and normalized traces (lower panel) illustrate Bay K8644 effects on the peak current and inactivation, respectively.

(E) Exemplar normalized Ba^{2+} currents from *Xenopus* oocytes expressing $Ca_V1.2$ or the indicated mutants, in response to a +20 mV depolarization in absence (black) or in presence of 5 μM Bay K8644 (blue).

(F) Ratio of Ca^{2+} current amplitudes in presence, I_{Ca}(Bay K), and in absence, I_{Ca}, of Bay K8644; n = 6–7.

(G and H) Percentage of inactivation 300 ms post-depolarization (t_{i300}) in absence (dark bars) and presence of Bay K8644 (light bars) using (G) Ca^{2+} or (H) Ba^{2+} as charge carrier. *p < 0.01 and **p < 0.001 compared to the same construct without Bay K8644; n = 6–11.

(I) Difference in t_{i300} induced by Bay K8644 in Ca^{2+}(dark bars) and Ba^{2+} (light bars).

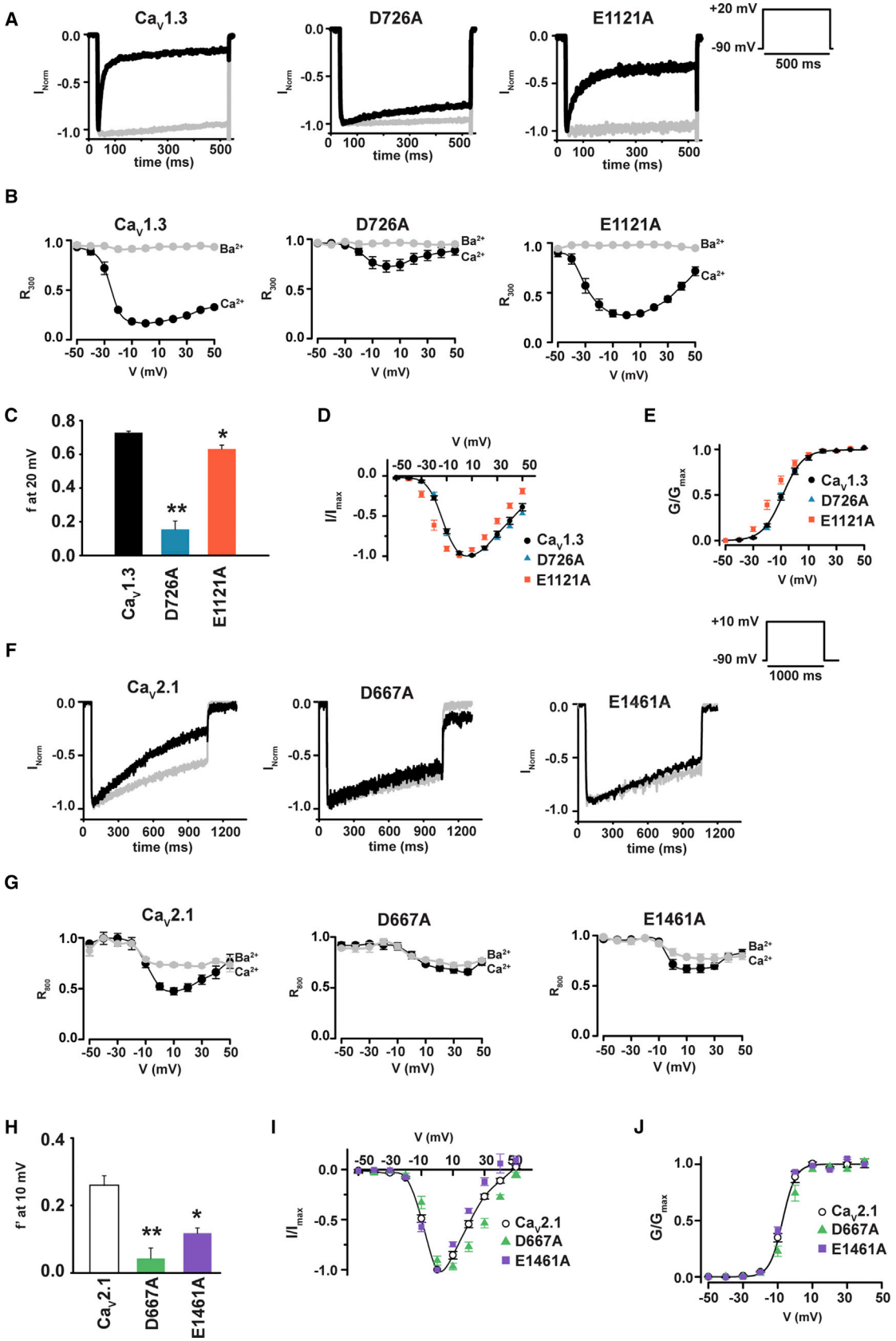

(legend on next page)

mutant (Figures 5C–5E), indicating that the DI (+1) site aspartate was unable to restore CDI in the face of the loss of the aspartate at the DII (+1) position. By contrast, exchange of the SF (+1) aspartate from the DII to DIII positions, $DIII_{Asp,}$ or from the DII to DIV positions, DIV_{Asp}, resulted in complete or near complete CDI restoration, respectively (Figures 5C–5E). These results demonstrate the ability of a SF (+1) aspartate to preserve CDI when located on DIII or DIV but not DI. To test whether reduced Ca^{2+} influx was the cause of the compromised CDI in DI_{Asp}, we examined the consequences of Bay K8644-enhanced Ca^{2+} influx on the SF (+1) swap mutants. Bay K8644 application increased Ca^{2+} currents by ~2-fold in all three (+1) swap mutants, similar to results on other SF mutants (Figures 3C, 3F, and 3G), but failed to enhance CDI in the channel having reduced CDI, DI_{Asp} (Figures S6A, S6C, and S6D). Studies using Ba^{2+} showed that, as with our other SF (+1) Bay K8644 experiments (Figure 3), inactivation is increased in a Ca^{2+}-independent manner (Figures S6B, S6E, and S6F). These results indicate that reduced CDI of DI_{Asp} is not caused by insufficient Ca^{2+} influx but is linked to a change in the ability of the SF to reach an inactivated state. The preservation of CDI in the $DIII_{Asp}$ and DIV_{Asp} swaps demonstrates that the single changes at DII (+1), D707G and D707A, do not preclude CDI provided that either the DIII or DIV domain provides the SF position (+1) negative charge. The fact that CDI occurs only when the (+1) negative charge resides on DII, DIII, or DIV, but not DI, supports the idea of asymmetric functional roles for the four elements of the SF (Ellinor et al., 1995; Parent and Gopalakrishnan, 1995; Yang et al., 1993) and indicates that the mere presence of a negative charge at the SF (+1) level is insufficient to support CDI.

To probe whether the swap mutations affected the ability of the channel to bind Ca^{2+}, we measured Ca^{2+} block of Li^{+} currents (Shaya et al., 2014; Yang et al., 1993). Interestingly, all three aspartate-swap mutants behaved identically to $Ca_V1.2$, indicating that the affinity for Ca^{2+} was preserved regardless of the domain that housed the (+1) aspartate (Figure 5F). This result contrasts the reduction in Ca^{2+} binding caused by the single-point mutants at the DII (+1) position (Figure 5F) (Shaya et al., 2014). The observation that Ca^{2+} binding is preserved when the aspartate is placed at any of the four possible site (+1) positions contrasts with the domain selective results for CDI that these mutants cause. This finding indicates that the involvement of the SF in CDI is not strictly related to its ability to bind Ca^{2+}. These results together with the differential contributions of the individual (+1) sites to CDI support the idea that the SF has a direct role in CDI.

DISCUSSION

CDI is an essential feature of high voltage-activated Ca_Vs (Ca_V1s and Ca_V2s) that serves as an activity-dependent autoregulatory mechanism for limiting Ca^{2+} influx (Christel and Lee, 2011; Dunlap, 2007; Liang et al., 2003; Simms and Zamponi, 2014). This process contributes to autism (Limpitikul et al., 2016), vision (Singh et al., 2006), and cardiac action potential duration (Alseikhan et al., 2002; Dick et al., 2016; Mahajan et al., 2008; Morotti et al., 2012; Splawski et al., 2004, 2005) and is impacted by alternative splicing (Bartels et al., 2018; Shen et al., 2006; Tan et al., 2011), RNA editing (Huang et al., 2012), as well as mutations in CaM associated with long QT syndrome (Limpitikul et al., 2014, 2017). Because CDI is central to both the biophysical and physiological functions of Ca_Vs, its molecular origins have been extensively investigated, especially from the vantage point of the intracellular, CaM-based sensor and the role of the IQ domain (Ben-Johny and Yue, 2014; Minor and Findeisen, 2010; Kim et al., 2008, 2010; Mori et al., 2008; Van Petegem et al., 2005). Although the involvement of this CaM-based sensor in CDI is firmly established, how conformational changes of this cytoplasmic element result in the cessation of ion flow through the channel and the exact CDI endpoint have remained unresolved (Babich et al., 2007; Barrett and Tsien, 2008; Cens et al., 2006; Findeisen and Minor, 2009; Kim et al., 2004; Tadross et al., 2010). Our observations provide the first evidence that the Ca_V SF is a central element of the CDI mechanism and constitutes the CDI gate.

Three Ca_V channel intracellular elements contribute to CDI: the N-terminal cytoplasmic domain (Ben Johny et al., 2013; Dick et al., 2008; Ivanina et al., 2000; Tadross et al., 2008), the $Ca_V\beta$/I-II loop complex (Almagor et al., 2012; Findeisen and Minor, 2009), and the C-terminal tail:CaM complex (Ben-Johny and Yue, 2014; Minor and Findeisen, 2010; Kim et al., 2008, 2010; Lee et al., 1999; Mori et al., 2008; Peterson et al., 1999; Van Petegem et al., 2005; Zühlke et al., 1999), with the C-terminal tail:CaM complex serving as the Ca^{2+} sensor that initiates CDI. Given this functionally interconnected network of domains that influence CDI, there has been an ongoing search to identify the molecular endpoints of Ca_V CDI (Barrett and Tsien, 2008; Benmocha Guggenheimer et al., 2016; Tadross et al., 2010). There has been much focus on the S6 pore lining helices as a candidate for the CDI endpoint (Benmocha Guggenheimer et al., 2016; Raybaud et al., 2006; Tadross et al., 2010; Tadross and Yue, 2010), as these transmembrane helices form the channel intracellular gate (Wu et al., 2015, 2016) and are directly linked to two of the three domains that affect CDI. Given the involvement of many channel parts in CDI, an allosteric framework has been

Figure 4. Domain II SF Mutations Reduce CDI in $Ca_V1.3$ and $Ca_V2.1$

(A) Exemplar normalized recordings at +20 mV in Ca^{2+} (black) or Ba^{2+} (gray) from HEK293 cells expressing $Ca_V1.3$ or the indicated mutants.

(B) Fractional current remaining 300 ms post-depolarization (R_{300}) as a function of the membrane potential for (A).

(C) Average f values at +20 mV. *$p < 0.01$ and **$p < 0.001$ compared to $Ca_V1.3$.

(D) I–V relationships for $Ca_V1.3$ (black circles), $Ca_V1.3$ D707A (blue triangles), and $Ca_V1.3$ E1121A (red orange squares).

(E) Voltage-dependent activation curves for the indicated channels. Symbols are as in (D).

(F) Exemplar normalized recordings at +10 mV in Ca^{2+} (black) or Ba^{2+} (gray) from HEK293 cells expressing $Ca_V2.1$ or the indicated mutants.

(G) Fractional current remaining 800 ms post-depolarization (R_{800}) as a function of the membrane potential for (F).

(H) Average f′ values at +10 mV, where is f′ the difference between Ca^{2+} and Ba^{2+} R_{800} values. *$p < 0.01$ and **$p < 0.001$ compared to $Ca_V2.1$.

(I) I–V relationships for $Ca_V2.1$ (open circles), $Ca_V2.1$ D667A (green triangles), and $Ca_V2.1$ E1461A (purple squares).

(J) Voltage-dependent activation curves for the indicated channels. Symbols are as in (I).

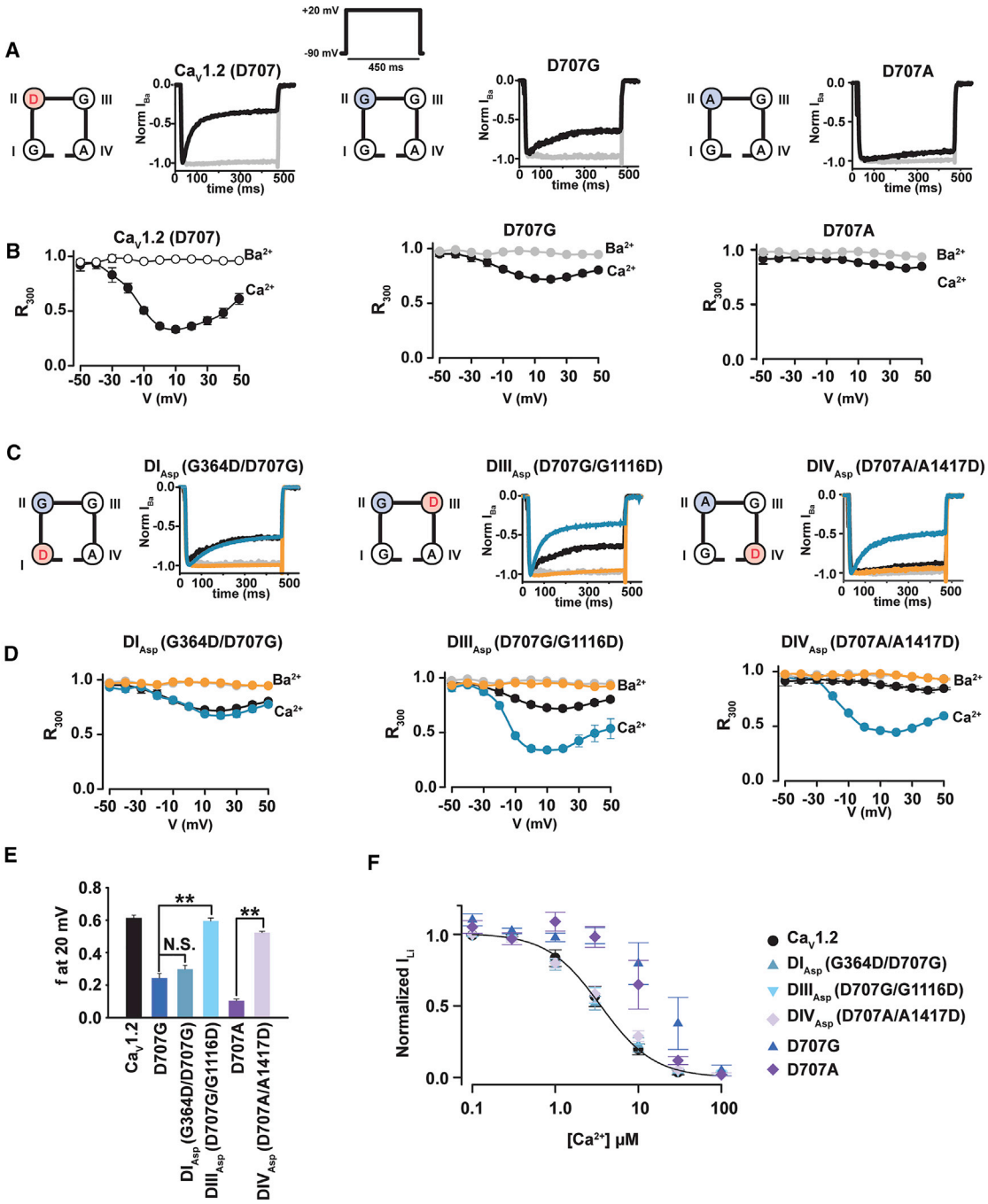

Figure 5. Ca$_V$1.2 CDI Requires a Negative Charge at the DII, DIII, or DIV SF (+1) Position

(A) Exemplar normalized recordings at +20 mV in Ca^{2+} (black) or Ba^{2+} (gray) from *Xenopus* oocytes expressing the Ca$_V$1.2 or the indicated mutants.

(B) Fractional current remaining 300 ms post-depolarization (R_{300}) as a function of the membrane potential for channels in (A). Data in (A) and (B) are identical to Figures 1A and 1B.

(C) Exemplar normalized recordings at +20 mV in Ca^{2+} (blue) or Ba^{2+} (orange) from *Xenopus* oocytes expressing the indicated Ca$_V$1.2 mutants moving the negative charge at the (+1) position of the selectivity filter from domain II to domains I, III, or IV. Ca^{2+} (black) and Ba^{2+} (gray) currents from Ca$_V$1.2 are shown for comparison.

(D) Fractional current remaining 300 ms post-depolarization (R_{300}) as a function of the membrane potential for channels in (C).

(E) Average f values at 20 mV. **$p < 0.001$ compared to the corresponding single mutant.

(F) Dose-response curves for Ca^{2+} block of Li^+ currents for Ca$_V$1.2, DI_{Asp} G364D/D707G (blue triangles), $DIII_{Asp}$ D707G/G1116D (inverted blue triangles), and DIV_{Asp} D707A/A1417D (lavender diamonds). Each data point at each Ca^{2+} concentration is normalized to the current at 3 nM Ca^{2+} and averaged for n = 7–9 oocytes.

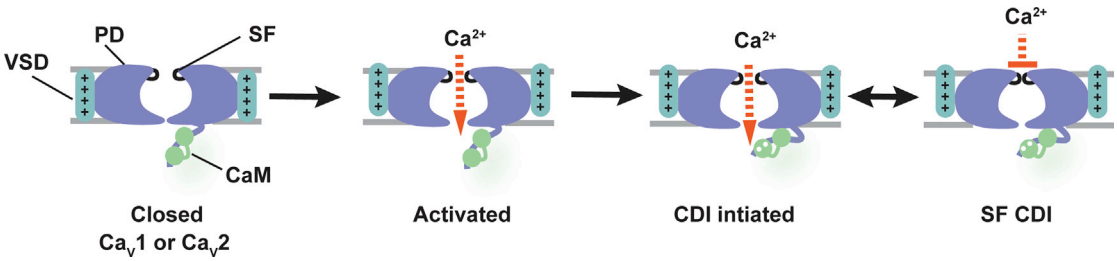

Figure 6. Ca_V CDI Model

Closed channels (left) are activated by depolarization that includes voltage sensor domain (VSD) activation and pore opening. Flow of Ca^{2+} through the channel leads to Ca^{2+} (white circles) binding to CaM (green) that initiates CDI. CDI results in a selectivity filter (SF) conformational change that obstructs ion flow. Pore domain, PD (violet), voltage sensor domain, VSD (cyan), and SF (black) are labeled. Gray bars indicate membrane. Other intracellular elements that affect CDI such as the N-terminal cytoplasmic domain and $Ca_V\beta$/I-II loop complex are not shown.

used to try to understand the actions of disease mutants on CDI (Dick et al., 2016; Limpitikul et al., 2016; Tadross et al., 2010). An alternative proposal is that the SF may participate in CDI through an ion-blocking model in which Ca^{2+}affinity is increased in the inactivated state (Babich et al., 2007). Our observations that SF DII (+1) site mutations such as D707A eliminate CDI but spare biophysical parameters related to the activation process are inconsistent with the proposal that the activation gate formed by S6 is the CDI endpoint (Tadross et al., 2010). Nevertheless, S6 is likely to be critical for coupling to the various intracellular domains that contribute to CDI and may mediate direct coupling between the activation gate and the SF-based CDI gate, similar to its role in other VGIC superfamily members (Ader et al., 2009; Cuello et al., 2017; Imai et al., 2010; Panyi and Deutsch, 2006; Peters et al., 2013). Further, in contrast to the proposal that CDI occurs through an increased affinity of the SF for Ca^{2+} (Babich et al., 2007), we find that mutations that remove the aspartate at the SF DII (+1) site can have identical Ca^{2+} affinities but exhibit very different degrees of CDI (Figures 1 and 5) (Shaya et al., 2014). Together, our findings establish that the Ca_V SF serves as the CDI gate and recast the paradigm for understanding the Ca_V CDI mechanism with a focus on the SF.

The pore domain of all VGIC superfamily members is made from four subunits arranged around the central ion-conducting pore (Yu et al., 2005) that share a common architectural fold comprising two transmembrane helices, the SF, and a short pore helix that supports the SF architecture (Catterall et al., 2017; Payandeh and Minor, 2015). Within the context of this shared architecture, studies of diverse VGIC superfamily members have begun to uncover a central role for SF in inactivation mechanisms, being best characterized in diverse potassium channel types including: KcsA (Cuello et al., 2010, 2017), Kvs (Liu et al., 1996; López-Barneo et al., 1993; Ogielska and Aldrich, 1999; Peters et al., 2013), and K_{2P}s (Bagriantsev et al., 2011; Cohen et al., 2008; Lolicato et al., 2017; Piechotta et al., 2011; Schewe et al., 2016). Additionally, structural observations of asymmetric $BacNa_V$ SF conformations (Catterall et al., 2017; Payandeh et al., 2012) and functional studies of SF (+4) position mutants (Pavlov et al., 2005) have suggested a role for the SF in $BacNa_V$ VDI that may be shared with eukaryotic Na_Vs and Ca_Vs (Catterall et al., 2017). Studies of members of the TRP channel branch, TRPV1 (Cao et al., 2013; Steinberg et al., 2017) and TRPM4 (Autzen et al., 2018), also support the idea that the SF constitutes a gate. Hence, the discovery that Ca_V CDI also relies on a SF-based mechanism sets Ca_Vs squarely within the growing list of VGICs in which SF-based gating is central to function. The apparent widespread role of the SF in the inactivation processes of VGIC superfamily members suggests that these SF-based inactivation mechanisms capitalize on a fundamental pore domain (PD) property that predates the evolutionary divergence in ion selectivity and gating cue responses among the VGIC superfamily branches. This prevalence of SF-based inactivation mechanisms seems likely to have its origins in the shared ancient structure that forms the PD.

Elements from the cytoplasmic side of the channel drive conformational changes that stop ion permeation for both CDI and VDI. Whether Ca_V CDI and VDI share a common mechanism has been unresolved (Barrett and Tsien, 2008; Cens et al., 2006; Findeisen and Minor, 2009; Kim et al., 2004; Tadross et al., 2010). Our studies support the idea that both processes involve the SF. Notably, we find that there are selective effects on CDI or VDI depending on which parts of the SF structure are altered (Figures 1 and S4), supporting the idea that CDI and VDI have different endpoints even though they are affected by common channel elements (Barrett and Tsien, 2008; Findeisen and Minor, 2009; Tadross et al., 2010). The VDI effects match those reported for $BacNa_V$s (Pavlov et al., 2005) and support the idea that there is a common SF-based mechanism underlying VDI in $BacNa_V$s, Ca_Vs, and Na_Vs (Catterall et al., 2017). Considering our new findings of the importance of the SF in CDI together with prior cytoplasmic domain studies (Almagor et al., 2012; Ben Johny et al., 2013; Dick et al., 2008; Findeisen and Minor, 2009; Ivanina et al., 2000; Kim et al., 2008, 2010; Lee et al., 1999; Mori et al., 2008; Peterson et al., 1999; Tadross et al., 2008; Van Petegem et al., 2005; Zühlke et al., 1999), we propose the following model in which SF conformational changes constitute the end stage of a CDI process that is initiated by CaM on the cytoplasmic side of the channel (Figure 6). Upon activation by voltage, Ca^{2+} influx through the channel is sensed by CaM and initiates a set of conformational rearrangements that end with a conformational change in the SF that stops ion flow. Although the exact conformational changes underling Ca_V SF inactivation and complete accounting of the residues involved remain to be elaborated and ultimately will require structural studies of the channel

trapped in various states, our data indicate that this process exploits the previously identified functional asymmetry in the Ca_V SF (Ellinor et al., 1995; Parent and Gopalakrishnan, 1995; Yang et al., 1993). In this regard, it is interesting to note that the SF DII (+1) aspartate seems capable of making interactions that involve other SF domain residues (Cheng et al., 2010) and that we can restore CDI to DII (+1) SF mutants by supplying an aspartate at the equivalent site in two of the three other domains (Figure 5).

Our studies provide clear evidence that the Ca_V SF plays a central role in the CDI process by forming the CDI gate. The evidence for this Ca_V SF gate, together with the presence of an inner gate formed by the S6 helices (Benmocha Guggenheimer et al., 2016; Raybaud et al., 2006; Tadross et al., 2010; Tadross and Yue, 2010; Wu et al., 2015, 2016), establishes that Ca_Vs use two gates to control their activity, similar to other VGIC superfamily members (Autzen et al., 2018; Cao et al., 2013; Cuello et al., 2017; Steinberg et al., 2017). This finding creates a new framework for addressing how the two Ca_V gates interact, whether they are coupled in a manner similar to structurally related potassium channels (Cuello et al., 2017), whether there are commonalities in SF-based inactivation mechanisms between channels that have wide SFs such as Ca_Vs versus those that intimately contact the permeant ions such as potassium channels (Cuello et al., 2017), and how the intracellular components that contribute to CDI (Almagor et al., 2012; Ben Johny et al., 2013; Ben-Johny and Yue, 2014; Dick et al., 2008; Findeisen and Minor, 2009; Minor and Findeisen, 2010; Ivanina et al., 2000; Kim et al., 2008, 2010; Lee et al., 1999; Mori et al., 2008; Peterson et al., 1999; Tadross et al., 2008; Van Petegem et al., 2005; Zühlke et al., 1999) affect structural transitions in the SF gate. Such issues may be important for understanding how Ca_V disease mutations that impact CDI act (Dick et al., 2016; Limpitikul et al., 2014, 2016, 2017; Singh et al., 2006; Splawski et al., 2004, 2005) and how such functional defects may be overcome by pharmacological intervention.

STAR★METHODS

Detailed methods are provided in the online version of this paper and include the following:

- KEY RESOURCES TABLE
- CONTACT FOR REAGENT AND RESOURCE SHARING
- EXPERIMENTAL MODEL AND SUBJECT DETAILS
  - Oocytes collection
  - Cell Culture
- METHOD DETAILS
  - Molecular Biology
  - Two-electrode voltage clamp electrophysiology
  - Whole-cell Patch-clamp electrophysiology
  - Single-channel recordings
  - Data Analysis
- QUANTIFICATION AND STATISTICAL ANALYSIS

SUPPLEMENTAL INFORMATION

Supplemental Information includes six figures and can be found with this article online at https://doi.org/10.1016/j.neuron.2019.01.011.

ACKNOWLEDGMENTS

We thank M. Grabe and L. Jan for comments on the manuscript. This work was supported by grant NIH-NHLBI R01-HL080050 to D.L.M. and a Marcel Bleustein-Blanchet Foundation fellowship to F.A.-A.

AUTHOR CONTRIBUTIONS

F.A.-A., F.F., and D.L.M. conceived the study and designed the experiments. F.A.-A., F.F., and N.D.R. performed two-electrode voltage-clamp electrophysiology experiments. F.A.-A. and N.D.R. performed whole-cell patch-clamp electrophysiology experiments. F.A.-A. performed single-channel experiments and analyzed all the electrophysiology data. F.A.-A. and F.F. performed molecular biology experiments. D.L.M. analyzed data and provided guidance and support. F.A.-A. and D.L.M. wrote the paper.

DECLARATION OF INTERESTS

The authors declare no competing interests.

Received: June 15, 2018
Revised: November 12, 2018
Accepted: December 31, 2018
Published: February 4, 2019

REFERENCES

Adams, P.J., Ben-Johny, M., Dick, I.E., Inoue, T., and Yue, D.T. (2014). Apocalmodulin itself promotes ion channel opening and Ca(2+) regulation. Cell *159*, 608–622.

Ader, C., Schneider, R., Hornig, S., Velisetty, P., Vardanyan, V., Giller, K., Ohmert, I., Becker, S., Pongs, O., and Baldus, M. (2009). Coupling of activation and inactivation gate in a K+-channel: Potassium and ligand sensitivity. EMBO J. *28*, 2825–2834.

Almagor, L., Chomsky-Hecht, O., Ben-Mocha, A., Hendin-Barak, D., Dascal, N., and Hirsch, J.A. (2012). The role of a voltage-dependent Ca2+ channel intracellular linker: A structure-function analysis. J. Neurosci. *32*, 7602–7613.

Alseikhan, B.A., DeMaria, C.D., Colecraft, H.M., and Yue, D.T. (2002). Engineered calmodulins reveal the unexpected eminence of Ca2+ channel inactivation in controlling heart excitation. Proc. Natl. Acad. Sci. USA *99*, 17185–17190.

Arrigoni, C., Rohaim, A., Shaya, D., Findeisen, F., Stein, R.A., Nurva, S.R., Mishra, S., Mchaourab, H.S., and Minor, D.L., Jr. (2016). Unfolding of a temperature-sensitive domain controls voltage-gated channel activation. Cell *164*, 922–936.

Autzen, H.E., Myasnikov, A.G., Campbell, M.G., Asarnow, D., Julius, D., and Cheng, Y. (2018). Structure of the human TRPM4 ion channel in a lipid nanodisc. Science *359*, 228–232.

Babich, O., Isaev, D., and Shirokov, R. (2005). Role of extracellular Ca2+ in gating of CaV1.2 channels. J. Physiol. *565*, 709–715.

Babich, O., Matveev, V., Harris, A.L., and Shirokov, R. (2007). Ca2+-dependent inactivation of CaV1.2 channels prevents Gd3+ block: does Ca2+ block the pore of inactivated channels? J. Gen. Physiol. *129*, 477–483.

Bagriantsev, S.N., Peyronnet, R., Clark, K.A., Honoré, E., and Minor, D.L., Jr. (2011). Multiple modalities converge on a common gate to control K2P channel function. EMBO J. *30*, 3594–3606.

Barrett, C.F., and Tsien, R.W. (2008). The Timothy syndrome mutation differentially affects voltage- and calcium-dependent inactivation of CaV1.2 L-type calcium channels. Proc. Natl. Acad. Sci. USA *105*, 2157–2162.

Bartels, P., Yu, D., Huang, H., Hu, Z., Herzig, S., and Soong, T.W. (2018). Alternative splicing at N terminus and domain I modulates $Ca_V1.2$ inactivation and surface expression. Biophys. J. *114*, 2095–2106.

Ben-Johny, M., and Yue, D.T. (2014). Calmodulin regulation (calmodulation) of voltage-gated calcium channels. J. Gen. Physiol. *143*, 679–692.

Ben Johny, M., Yang, P.S., Bazzazi, H., and Yue, D.T. (2013). Dynamic switching of calmodulin interactions underlies Ca2+ regulation of CaV1.3 channels. Nat. Commun. *4*, 1717.

Benmocha Guggenheimer, A., Almagor, L., Tsemakhovich, V., Tripathy, D.R., Hirsch, J.A., and Dascal, N. (2016). Interactions between N and C termini of α1C subunit regulate inactivation of CaV1.2 L-type Ca(2+) channel. Channels (Austin) *10*, 55–68.

Bock, G., Gebhart, M., Scharinger, A., Jangsangthong, W., Busquet, P., Poggiani, C., Sartori, S., Mangoni, M.E., Sinnegger-Brauns, M.J., Herzig, S., et al. (2011). Functional properties of a newly identified C-terminal splice variant of Cav1.3 L-type Ca2+ channels. J. Biol. Chem. *286*, 42736–42748.

Campiglio, M., and Flucher, B.E. (2015). The role of auxiliary subunits for the functional diversity of voltage-gated calcium channels. J. Cell. Physiol. *230*, 2019–2031.

Cao, E., Liao, M., Cheng, Y., and Julius, D. (2013). TRPV1 structures in distinct conformations reveal activation mechanisms. Nature *504*, 113–118.

Catterall, W.A. (2011). Voltage-gated calcium channels. Cold Spring Harb. Perspect. Biol. *3*, a003947.

Catterall, W.A., Wisedchaisri, G., and Zheng, N. (2017). The chemical basis for electrical signaling. Nat. Chem. Biol. *13*, 455–463.

Cens, T., Restituito, S., Galas, S., and Charnet, P. (1999). Voltage and calcium use the same molecular determinants to inactivate calcium channels. J. Biol. Chem. *274*, 5483–5490.

Cens, T., Rousset, M., Leyris, J.P., Fesquet, P., and Charnet, P. (2006). Voltage- and calcium-dependent inactivation in high voltage-gated Ca(2+) channels. Prog. Biophys. Mol. Biol. *90*, 104–117.

Chen, Y.H., Li, M.H., Zhang, Y., He, L.L., Yamada, Y., Fitzmaurice, A., Shen, Y., Zhang, H., Tong, L., and Yang, J. (2004). Structural basis of the alpha1-beta subunit interaction of voltage-gated Ca2+ channels. Nature *429*, 675–680.

Cheng, R.C., Tikhonov, D.B., and Zhorov, B.S. (2010). Structural modeling of calcium binding in the selectivity filter of the L-type calcium channel. Eur. Biophys. J. *39*, 839–853.

Christel, C., and Lee, A. (2011). Ca(2+)-dependent modulation of voltage-gated Ca(2+) channels. Biochim. Biophys. Acta *1820*, 1243–1252.

Clapham, D.E. (2007). Calcium signaling. Cell *131*, 1047–1058.

Cohen, A., Ben-Abu, Y., Hen, S., and Zilberberg, N. (2008). A novel mechanism for human K2P2.1 channel gating. Facilitation of C-type gating by protonation of extracellular histidine residues. J. Biol. Chem. *283*, 19448–19455.

Cuello, L.G., Jogini, V., Cortes, D.M., and Perozo, E. (2010). Structural mechanism of C-type inactivation in K(+) channels. Nature *466*, 203–208.

Cuello, L.G., Cortes, D.M., and Perozo, E. (2017). The gating cycle of a K^+ channel at atomic resolution. eLife *6*. Published online November 22, 2017. https://doi.org/10.7554/eLife.28032.

De Waard, M., and Campbell, K.P. (1995). Subunit regulation of the neuronal alpha 1A Ca2+ channel expressed in Xenopus oocytes. J. Physiol. *485*, 619–634.

DeMaria, C.D., Soong, T.W., Alseikhan, B.A., Alvania, R.S., and Yue, D.T. (2001). Calmodulin bifurcates the local Ca2+ signal that modulates P/Q-type Ca2+ channels. Nature *411*, 484–489.

Dick, I.E., Tadross, M.R., Liang, H., Tay, L.H., Yang, W., and Yue, D.T. (2008). A modular switch for spatial Ca2+ selectivity in the calmodulin regulation of CaV channels. Nature *451*, 830–834.

Dick, I.E., Joshi-Mukherjee, R., Yang, W., and Yue, D.T. (2016). Arrhythmogenesis in Timothy syndrome is associated with defects in Ca(2+)-dependent inactivation. Nat. Commun. *7*, 10370.

Doering, C.J., Hamid, J., Simms, B., McRory, J.E., and Zamponi, G.W. (2005). Cav1.4 encodes a calcium channel with low open probability and unitary conductance. Biophys. J. *89*, 3042–3048.

Dolphin, A.C. (2016). Voltage-gated calcium channels and their auxiliary subunits: physiology and pathophysiology and pharmacology. J. Physiol. *594*, 5369–5390.

Dunlap, K. (2007). Calcium channels are models of self-control. J. Gen. Physiol. *129*, 379–383.

Ellinor, P.T., Yang, J., Sather, W.A., Zhang, J.F., and Tsien, R.W. (1995). Ca2+ channel selectivity at a single locus for high-affinity Ca2+ interactions. Neuron *15*, 1121–1132.

Fallon, J.L., Halling, D.B., Hamilton, S.L., and Quiocho, F.A. (2005). Structure of calmodulin bound to the hydrophobic IQ domain of the cardiac Ca(v)1.2 calcium channel. Structure *13*, 1881–1886.

Fallon, J.L., Baker, M.R., Xiong, L., Loy, R.E., Yang, G., Dirksen, R.T., Hamilton, S.L., and Quiocho, F.A. (2009). Crystal structure of dimeric cardiac L-type calcium channel regulatory domains bridged by Ca2+* calmodulins. Proc. Natl. Acad. Sci. USA *106*, 5135–5140.

Findeisen, F., and Minor, D.L., Jr. (2009). Disruption of the IS6-AID linker affects voltage-gated calcium channel inactivation and facilitation. J. Gen. Physiol. *133*, 327–343.

Halling, D.B., Aracena-Parks, P., and Hamilton, S.L. (2006). Regulation of voltage-gated Ca2+ channels by calmodulin. Sci. STKE *2006*, er1.

Hamill, O.P., Marty, A., Neher, E., Sakmann, B., and Sigworth, F.J. (1981). Improved patch-clamp techniques for high-resolution current recording from cells and cell-free membrane patches. Pflugers Arch. *391*, 85–100.

Hess, P., Lansman, J.B., and Tsien, R.W. (1984). Different modes of Ca channel gating behaviour favoured by dihydropyridine Ca agonists and antagonists. Nature *311*, 538–544.

Huang, H., Tan, B.Z., Shen, Y., Tao, J., Jiang, F., Sung, Y.Y., Ng, C.K., Raida, M., Köhr, G., Higuchi, M., et al. (2012). RNA editing of the IQ domain in Ca(v)1.3 channels modulates their Ca^{2+}-dependent inactivation. Neuron *73*, 304–316.

Huang, H., Yu, D., and Soong, T.W. (2013). C-terminal alternative splicing of CaV1.3 channels distinctively modulates their dihydropyridine sensitivity. Mol. Pharmacol. *84*, 643–653.

Imai, S., Osawa, M., Takeuchi, K., and Shimada, I. (2010). Structural basis underlying the dual gate properties of KcsA. Proc. Natl. Acad. Sci. USA *107*, 6216–6221.

Ivanina, T., Blumenstein, Y., Shistik, E., Barzilai, R., and Dascal, N. (2000). Modulation of L-type Ca2+ channels by gbeta gamma and calmodulin via interactions with N and C termini of alpha 1C. J. Biol. Chem. *275*, 39846–39854.

Kim, M.S., Morii, T., Sun, L.X., Imoto, K., and Mori, Y. (1993). Structural determinants of ion selectivity in brain calcium channel. FEBS Lett. *318*, 145–148.

Kim, J., Ghosh, S., Nunziato, D.A., and Pitt, G.S. (2004). Identification of the components controlling inactivation of voltage-gated Ca2+ channels. Neuron *41*, 745–754.

Kim, E.Y., Rumpf, C.H., Fujiwara, Y., Cooley, E.S., Van Petegem, F., and Minor, D.L., Jr. (2008). Structures of CaV2 Ca2+/CaM-IQ domain complexes reveal binding modes that underlie calcium-dependent inactivation and facilitation. Structure *16*, 1455–1467.

Kim, E.Y., Findeisen, F., and Minor, D.L., Jr. (2010). Calmodulin interactions with CaV1 and CaV2 voltage-gated calcium channel IQ domains. In Handbook of Metalloproteins, A. Messerschmidt, ed. (John Wiley).

Koishi, R., Xu, H., Ren, D., Navarro, B., Spiller, B.W., Shi, Q., and Clapham, D.E. (2004). A superfamily of voltage-gated sodium channels in bacteria. J. Biol. Chem. *279*, 9532–9538.

Lee, A., Wong, S.T., Gallagher, D., Li, B., Storm, D.R., Scheuer, T., and Catterall, W.A. (1999). Ca2+/calmodulin binds to and modulates P/Q-type calcium channels. Nature *399*, 155–159.

Lee, A., Zhou, H., Scheuer, T., and Catterall, W.A. (2003). Molecular determinants of Ca2+/calmodulin-dependent regulation of Cav2.1 channels. Proc. Natl. Acad. Sci. USA *100*, 16059–16064.

Liang, H., DeMaria, C.D., Erickson, M.G., Mori, M.X., Alseikhan, B.A., and Yue, D.T. (2003). Unified mechanisms of Ca2+ regulation across the Ca2+ channel family. Neuron *39*, 951–960.

Limpitikul, W.B., Dick, I.E., Joshi-Mukherjee, R., Overgaard, M.T., George, A.L., Jr., and Yue, D.T. (2014). Calmodulin mutations associated with long QT syndrome prevent inactivation of cardiac L-type Ca(2+) currents and

promote proarrhythmic behavior in ventricular myocytes. J. Mol. Cell. Cardiol. *74*, 115–124.

Limpitikul, W.B., Dick, I.E., Ben-Johny, M., and Yue, D.T. (2016). An autism-associated mutation in CaV1.3 channels has opposing effects on voltage- and Ca(2+)-dependent regulation. Sci. Rep. *6*, 27235.

Limpitikul, W.B., Dick, I.E., Tester, D.J., Boczek, N.J., Limphong, P., Yang, W., Choi, M.H., Babich, J., DiSilvestre, D., Kanter, R.J., et al. (2017). A precision medicine approach to the rescue of function on malignant calmodulinopathic long-QT syndrome. Circ. Res. *120*, 39–48.

Liu, Y., Jurman, M.E., and Yellen, G. (1996). Dynamic rearrangement of the outer mouth of a K+ channel during gating. Neuron *16*, 859–867.

Lolicato, M., Arrigoni, C., Mori, T., Sekioka, Y., Bryant, C., Clark, K.A., and Minor, D.L., Jr. (2017). K_{2P}2.1 (TREK-1)-activator complexes reveal a cryptic selectivity filter binding site. Nature *547*, 364–368.

López-Barneo, J., Hoshi, T., Heinemann, S.H., and Aldrich, R.W. (1993). Effects of external cations and mutations in the pore region on C-type inactivation of Shaker potassium channels. Receptors Channels *1*, 61–71.

Mahajan, A., Sato, D., Shiferaw, Y., Baher, A., Xie, L.H., Peralta, R., Olcese, R., Garfinkel, A., Qu, Z., and Weiss, J.N. (2008). Modifying L-type calcium current kinetics: consequences for cardiac excitation and arrhythmia dynamics. Biophys. J. *94*, 411–423.

Mikala, G., Bahinski, A., Yatani, A., Tang, S., and Schwartz, A. (1993). Differential contribution by conserved glutamate residues to an ion-selectivity site in the L-type Ca2+ channel pore. FEBS Lett. *335*, 265–269.

Minor, D.L., Jr., and Findeisen, F. (2010). Progress in the structural understanding of voltage-gated calcium channel (CaV) function and modulation. Channels (Austin) *4*, 459–474.

Mori, M.X., Vander Kooi, C.W., Leahy, D.J., and Yue, D.T. (2008). Crystal structure of the CaV2 IQ domain in complex with Ca2+/calmodulin: high-resolution mechanistic implications for channel regulation by Ca2+. Structure *16*, 607–620.

Morotti, S., Grandi, E., Summa, A., Ginsburg, K.S., and Bers, D.M. (2012). Theoretical study of L-type Ca(2+) current inactivation kinetics during action potential repolarization and early afterdepolarizations. J. Physiol. *590*, 4465–4481.

Nanou, E., and Catterall, W.A. (2018). Calcium channels, synaptic plasticity, and neuropsychiatric disease. Neuron *98*, 466–481.

Noceti, F., Olcese, R., Qin, N., Zhou, J., and Stefani, E. (1998). Effect of bay K 8644 (-) and the beta2a subunit on Ca2+-dependent inactivation in alpha1C Ca2+ channels. J. Gen. Physiol. *111*, 463–475.

Ogielska, E.M., and Aldrich, R.W. (1999). Functional consequences of a decreased potassium affinity in a potassium channel pore. Ion interactions and C-type inactivation. J. Gen. Physiol. *113*, 347–358.

Olcese, R., Qin, N., Schneider, T., Neely, A., Wei, X., Stefani, E., and Birnbaumer, L. (1994). The amino terminus of a calcium channel beta subunit sets rates of channel inactivation independently of the subunit's effect on activation. Neuron *13*, 1433–1438.

Opatowsky, Y., Chen, C.C., Campbell, K.P., and Hirsch, J.A. (2004). Structural analysis of the voltage-dependent calcium channel beta subunit functional core and its complex with the alpha 1 interaction domain. Neuron *42*, 387–399.

Panyi, G., and Deutsch, C. (2006). Cross talk between activation and slow inactivation gates of Shaker potassium channels. J. Gen. Physiol. *128*, 547–559.

Parent, L., and Gopalakrishnan, M. (1995). Glutamate substitution in repeat IV alters divalent and monovalent cation permeation in the heart Ca2+ channel. Biophys. J. *69*, 1801–1813.

Pavlov, E., Bladen, C., Winkfein, R., Diao, C., Dhaliwal, P., and French, R.J. (2005). The pore, not cytoplasmic domains, underlies inactivation in a prokaryotic sodium channel. Biophys. J. *89*, 232–242.

Payandeh, J., and Minor, D.L., Jr. (2015). Bacterial voltage-gated sodium channels (BacNa(V)s) from the soil, sea, and salt lakes enlighten molecular mechanisms of electrical signaling and pharmacology in the brain and heart. J. Mol. Biol. *427*, 3–30.

Payandeh, J., Scheuer, T., Zheng, N., and Catterall, W.A. (2011). The crystal structure of a voltage-gated sodium channel. Nature *475*, 353–358.

Payandeh, J., Gamal El-Din, T.M., Scheuer, T., Zheng, N., and Catterall, W.A. (2012). Crystal structure of a voltage-gated sodium channel in two potentially inactivated states. Nature *486*, 135–139.

Peters, C.J., Fedida, D., and Accili, E.A. (2013). Allosteric coupling of the inner activation gate to the outer pore of a potassium channel. Sci. Rep. *3*, 3025.

Peterson, B.Z., DeMaria, C.D., Adelman, J.P., and Yue, D.T. (1999). Calmodulin is the Ca2+ sensor for Ca2+ -dependent inactivation of L-type calcium channels. Neuron *22*, 549–558.

Piechotta, P.L., Rapedius, M., Stansfeld, P.J., Bollepalli, M.K., Ehrlich, G., Andres-Enguix, I., Fritzenschaft, H., Decher, N., Sansom, M.S., Tucker, S.J., and Baukrowitz, T. (2011). The pore structure and gating mechanism of K2P channels. EMBO J. *30*, 3607–3619.

Raybaud, A., Dodier, Y., Bissonnette, P., Simoes, M., Bichet, D.G., Sauvé, R., and Parent, L. (2006). The role of the GX9GX3G motif in the gating of high voltage-activated Ca2+ channels. J. Biol. Chem. *281*, 39424–39436.

Ren, D., Navarro, B., Xu, H., Yue, L., Shi, Q., and Clapham, D.E. (2001). A prokaryotic voltage-gated sodium channel. Science *294*, 2372–2375.

Schewe, M., Nematian-Ardestani, E., Sun, H., Musinszki, M., Cordeiro, S., Bucci, G., de Groot, B.L., Tucker, S.J., Rapedius, M., and Baukrowitz, T. (2016). A non-canonical voltage-sensing mechanism controls gating in K2P K(+) channels. Cell *164*, 937–949.

Shaya, D., Kreir, M., Robbins, R.A., Wong, S., Hammon, J., Brüggemann, A., and Minor, D.L., Jr. (2011). Voltage-gated sodium channel (NaV) protein dissection creates a set of functional pore-only proteins. Proc. Natl. Acad. Sci. USA *108*, 12313–12318.

Shaya, D., Findeisen, F., Abderemane-Ali, F., Arrigoni, C., Wong, S., Nurva, S.R., Loussouarn, G., and Minor, D.L., Jr. (2014). Structure of a prokaryotic sodium channel pore reveals essential gating elements and an outer ion binding site common to eukaryotic channels. J. Mol. Biol. *426*, 467–483.

Shen, Y., Yu, D., Hiel, H., Liao, P., Yue, D.T., Fuchs, P.A., and Soong, T.W. (2006). Alternative splicing of the Ca(v)1.3 channel IQ domain, a molecular switch for Ca2+-dependent inactivation within auditory hair cells. J. Neurosci. *26*, 10690–10699.

Simms, B.A., and Zamponi, G.W. (2014). Neuronal voltage-gated calcium channels: structure, function, and dysfunction. Neuron *82*, 24–45.

Singh, A., Hamedinger, D., Hoda, J.C., Gebhart, M., Koschak, A., Romanin, C., and Striessnig, J. (2006). C-terminal modulator controls Ca2+-dependent gating of Ca(v)1.4 L-type Ca2+ channels. Nat. Neurosci. *9*, 1108–1116.

Singh, A., Gebhart, M., Fritsch, R., Sinnegger-Brauns, M.J., Poggiani, C., Hoda, J.C., Engel, J., Romanin, C., Striessnig, J., and Koschak, A. (2008). Modulation of voltage- and Ca2+-dependent gating of CaV1.3 L-type calcium channels by alternative splicing of a C-terminal regulatory domain. J. Biol. Chem. *283*, 20733–20744.

Splawski, I., Timothy, K.W., Sharpe, L.M., Decher, N., Kumar, P., Bloise, R., Napolitano, C., Schwartz, P.J., Joseph, R.M., Condouris, K., et al. (2004). Ca(V)1.2 calcium channel dysfunction causes a multisystem disorder including arrhythmia and autism. Cell *119*, 19–31.

Splawski, I., Timothy, K.W., Decher, N., Kumar, P., Sachse, F.B., Beggs, A.H., Sanguinetti, M.C., and Keating, M.T. (2005). Severe arrhythmia disorder caused by cardiac L-type calcium channel mutations. Proc. Natl. Acad. Sci. USA *102*, 8089–8096, discussion 8086–8088.

Stea, A., Tomlinson, W.J., Soong, T.W., Bourinet, E., Dubel, S.J., Vincent, S.R., and Snutch, T.P. (1994). Localization and functional properties of a rat brain alpha 1A calcium channel reflect similarities to neuronal Q- and P-type channels. Proc. Natl. Acad. Sci. USA *91*, 10576–10580.

Steinberg, X., Kasimova, M.A., Cabezas-Bratesco, D., Galpin, J.D., Ladron-de-Guevara, E., Villa, F., Carnevale, V., Islas, L., Ahern, C.A., and Brauchi, S.E. (2017). Conformational dynamics in TRPV1 channels reported by an

encoded coumarin amino acid. eLife *6*. Published online December 5, 2017. https://doi.org/10.7554/eLife.28626.

Stotz, S.C., Jarvis, S.E., and Zamponi, G.W. (2004). Functional roles of cytoplasmic loops and pore lining transmembrane helices in the voltage-dependent inactivation of HVA calcium channels. J. Physiol. *554*, 263–273.

Tadross, M.R., and Yue, D.T. (2010). Systematic mapping of the state dependence of voltage- and Ca2+-dependent inactivation using simple open-channel measurements. J. Gen. Physiol. *135*, 217–227.

Tadross, M.R., Dick, I.E., and Yue, D.T. (2008). Mechanism of local and global Ca2+ sensing by calmodulin in complex with a Ca2+ channel. Cell *133*, 1228–1240.

Tadross, M.R., Ben Johny, M., and Yue, D.T. (2010). Molecular endpoints of Ca2+/calmodulin- and voltage-dependent inactivation of Ca(v)1.3 channels. J. Gen. Physiol. *135*, 197–215.

Tadross, M.R., Tsien, R.W., and Yue, D.T. (2013). Ca2+ channel nanodomains boost local Ca2+ amplitude. Proc. Natl. Acad. Sci. USA *110*, 15794–15799.

Tan, B.Z., Jiang, F., Tan, M.Y., Yu, D., Huang, H., Shen, Y., and Soong, T.W. (2011). Functional characterization of alternative splicing in the C terminus of L-type CaV1.3 channels. J. Biol. Chem. *286*, 42725–42735.

Van Petegem, F., Clark, K.A., Chatelain, F.C., and Minor, D.L., Jr. (2004). Structure of a complex between a voltage-gated calcium channel beta-subunit and an alpha-subunit domain. Nature *429*, 671–675.

Van Petegem, F., Chatelain, F.C., and Minor, D.L., Jr. (2005). Insights into voltage-gated calcium channel regulation from the structure of the CaV1.2 IQ domain-Ca2+/calmodulin complex. Nat. Struct. Mol. Biol. *12*, 1108–1115.

Wu, J., Yan, Z., Li, Z., Yan, C., Lu, S., Dong, M., and Yan, N. (2015). Structure of the voltage-gated calcium channel Cav1.1 complex. Science *350*, aad2395.

Wu, J., Yan, Z., Li, Z., Qian, X., Lu, S., Dong, M., Zhou, Q., and Yan, N. (2016). Structure of the voltage-gated calcium channel Ca(v)1.1 at 3.6 Å resolution. Nature *537*, 191–196.

Xu, W., and Lipscombe, D. (2001). Neuronal Ca(V)1.3alpha(1) L-type channels activate at relatively hyperpolarized membrane potentials and are incompletely inhibited by dihydropyridines. J. Neurosci. *21*, 5944–5951.

Yang, J., Ellinor, P.T., Sather, W.A., Zhang, J.F., and Tsien, R.W. (1993). Molecular determinants of Ca2+ selectivity and ion permeation in L-type Ca2+ channels. Nature *366*, 158–161.

Yang, G., Shi, Y., Yu, J., Li, Y., Yu, L., Welling, A., Hofmann, F., Striessnig, J., Juntti-Berggren, L., Berggren, P.O., and Yang, S.N. (2015). CaV1.2 and CaV1.3 channel hyperactivation in mouse islet β cells exposed to type 1 diabetic serum. Cell. Mol. Life Sci. *72*, 1197–1207.

Yu, F.H., Yarov-Yarovoy, V., Gutman, G.A., and Catterall, W.A. (2005). Overview of molecular relationships in the voltage-gated ion channel superfamily. Pharmacol. Rev. *57*, 387–395.

Yue, L., Navarro, B., Ren, D., Ramos, A., and Clapham, D.E. (2002). The cation selectivity filter of the bacterial sodium channel, NaChBac. J. Gen. Physiol. *120*, 845–853.

Zamponi, G.W., Striessnig, J., Koschak, A., and Dolphin, A.C. (2015). The physiology, pathology, and pharmacology of voltage-gated calcium channels and their future therapeutic potential. Pharmacol. Rev. *67*, 821–870.

Zong, S., Zhou, J., and Tanabe, T. (1994). Molecular determinants of calcium-dependent inactivation in cardiac L-type calcium channels. Biochem. Biophys. Res. Commun. *201*, 1117–1123.

Zühlke, R.D., Pitt, G.S., Deisseroth, K., Tsien, R.W., and Reuter, H. (1999). Calmodulin supports both inactivation and facilitation of L-type calcium channels. Nature *399*, 159–162.

STAR★METHODS

KEY RESOURCES TABLE

REAGENT or RESOURCE	SOURCE	IDENTIFIER
Bacterial and Virus Strains		
Dh5α competent *E. coli*	MCLAB	Cat#DA-196
Chemicals, Peptides, and Recombinant Proteins		
ethylene glycol-bis(β-aminoethyl ether)-N,N,N',N'-tetraacetic acid (EGTA)	Sigma-Aldrich	Cat#E4378
1,2-Bis(2-aminophenoxy)ethane-N,N,N',N'-tetraacetic acid tetrakis (BAPTA)	Santa Cruz Biotechnology	Cat#sc-202076
Dulbecco's modified Eagle's medium (DMEM)	GIBCO	Cat#11965-092
fetal bovine serum (FBS)	GIBCO	Cat#16140-071
L-glutamine	GIBCO	Cat#25030-081
penicillin/streptomycin	UCSF Cell Culture Facility	Cat#CCFGK004-153K01
Lipofectamine 2000	Invitrogen	Cat#11668-019
Matrigel	BD Biosciences	Cat#354234
Critical Commercial Assays		
T7 mMessenger kit	Thermo Fisher Scientific	Cat# AM1344
QuikChange Site-Directed Mutagenesis Kit	Agilent	Cat#200515
Experimental Models: Cell Lines		
HEK293	ATCC	Cat#CRL-1573
Xenopus oocytes	This study	N/A
Experimental Models: Organisms/Strains		
Xenopus Laevis	Nasco	Cat# LM00531
Recombinant DNA		
human $Ca_V1.2$/pcDNA3.1	Findeisen and Minor, 2009	N/A
human $Ca_V1.2$ D707A/pcDNA3.1	Shaya et al., 2014	N/A
human $Ca_V1.2$ D707N/pcDNA3.1	Shaya et al., 2014	N/A
human $Ca_V1.2$ D707G/pcDNA3.1	Shaya et al., 2014	N/A
human $Ca_V1.2$ D707E/pcDNA3.1	This study	N/A
human $Ca_V1.2$ E1115A/pcDNA3.1	This study	N/A
human $Ca_V1.2$ D367A/pcDNA3.1	This study	N/A
human $Ca_V1.2$ E1119A/pcDNA3.1	This study	N/A
human $Ca_V1.2$ D1420A/pcDNA3.1	This study	N/A
human $Ca_V1.2$ G364D/D707G/pcDNA3.1	This study	N/A
human $Ca_V1.2$ D707G/G1116D/pcDNA3.1	This study	N/A
human $Ca_V1.2$ D707A/A1417D/pcDNA3.1	This study	N/A
rat $Ca_V1.3_{42a}$/pcDNA6/V5-His ABC	Xu and Lipscombe, 2001	Addgene#26577
rat $Ca_V1.3$ D726A/pcDNA6/V5-His ABC	This study	N/A
rat $Ca_V1.3$ E1121A/pcDNA6/V5-His ABC	This study	N/A
human $Ca_V2.1$/pcDNA3.1	Kim et al., 2008	N/A
human $Ca_V2.1$ D667A/pcDNA3.1	This study	N/A
human $Ca_V2.1$ E1461A/pcDNA3.1	This study	N/A
rat $Ca_V\beta_{2a}$/pTracer-CMV2-GFP	Findeisen and Minor, 2009	N/A
rabbit $Ca_V\beta_3$/pSport	This study	N/A
rabbit $Ca_V\alpha_2\delta$-1/pcDNA3.1	Findeisen and Minor, 2009	N/A
sv40 T-antigen/Bluescribe	addgene	Cat#21826

(*Continued on next page*)

Continued

REAGENT or RESOURCE	SOURCE	IDENTIFIER
Software and Algorithms		
pCLAMP 9	Molecular Devices	N/A
Clampfit 10	Molecular Devices	N/A
SigmaStat 3.1	Systat	N/A

CONTACT FOR REAGENT AND RESOURCE SHARING

Further information and requests for resources and reagents should be directed to and will be fulfilled by the Lead Contact, Daniel L. Minor, Jr. (daniel.minor@ucsf.edu).

EXPERIMENTAL MODEL AND SUBJECT DETAILS

Oocytes collection

Oocytes were harvested from female *Xenopus laevis* frogs purchased from Nasco and housed in the UCSF Laboratory Animal Resource Center (LARC) facilities. The use of these *Xenopus* oocytes was approved by IACUC (protocol approval # AN178461-01) and experiments were performed in accordance with University of California guidelines and regulations.

Cell Culture

Human embryonic kidney cells (HEK293) were purchased from ATCC (CRL-1573) and were grown at 37°C under 5% CO_2, in a Dulbecco's modified Eagle's medium (DMEM) supplemented with 10% fetal bovine serum (FBS), 10% L-glutamine, and antibiotics (100 IU mL−1 penicillin and 100 mg mL^{-1} streptomycin) (University of California, San Francisco Cell Culture Facility). The sex of cell line is not determined.

METHOD DETAILS

Molecular Biology

Human $Ca_V1.2$ (α_1C77, GenBank: Z34815), human $Ca_V2.1$ (α_1A, GenBank: NM_001127221.1), rat Cav1.3 (α_1D, GenBank: AF370009.1), rat $Ca_V\beta_{2a}$ (GenBank: NM_053851), rabbit $Ca_V\beta_3$ (GenBank: NM_001101715.2), and rabbit $Ca_V\alpha_2\delta$-1 (GenBank: NM_001082276.1) were used for both patch clamp and two-electrode voltage clamp experiments. $Ca_V1.2$ mutations were introduced by two separate PCR reactions. First the region of interest was PCR amplified using pcDNA3.1 Cav1.2 as template. The PCR product was then subcloned into pcDNA3.1 by restriction-ligation. The new plasmid containing the region of interest was then used as template to introduce the desired mutation using the QuikChange Site-Directed Mutagenesis Kit (Stratagene). The region of interest containing the desired mutation was then subcloned back into the pcDNA3.1 Cav1.2 to form the mutant full-length channel using the following restriction sites: NheI-HpaI, HpaI-PpuMI, KpnI-AgeI, and AgeI-FseI, for DI, DII, DIII, and DIV mutants, respectively. $Ca_V2.1$ and $Ca_V1.3$ mutants were made using the QuikChange Site-Directed Mutagenesis Kit (Agilent). All mutants were validated by complete sequencing of the genes encoding for the proteins of interest.

Two-electrode voltage clamp electrophysiology

Linearized cDNA was translated into capped mRNA using the T7 mMessenger kit (Ambion). We injected 50 nL of $Ca_V1.2\alpha1$, $Ca_V\beta_{2a}$ or $Ca_V\beta_3$ and $Ca_V\alpha_2\delta$-1 mRNA at a 1:1:1 molar ratio into *Xenopus* oocytes. Two-electrode voltage clamp experiments were performed 2–3 days post-injection.

Oocytes were injected with 50 nL of 100 mM BAPTA four minutes before recording, to minimize calcium-activated chloride currents as previously described (Findeisen and Minor, 2009). For recording of Ca^{2+} or Ba^{2+} currents, bath solutions contained 40 mM $CaCl_2$ or 40 mM $BaCl_2$, respectively, 50 mM NMDG-Cl, 1 mM KOH, 10 mM HEPES, adjusted to pH 7.4 with HNO_3. Measurements of Ca^{2+} block of Li^+ currents followed previously described protocols (Shaya et al., 2014). The bath solution contained 100 mM LiOH, $Ca(NO_3)_2$ at test concentrations between 3 nM and 100 μM, and 10 mM HEPES, adjusted to pH 7.4 with HNO_3. Ca^{2+} concentrations were verified using a Ca^{2+} electrode. A solution having a nominal 3 nM free Ca^{2+} concentration was used as control condition and contained 170 μM $Ca(NO_3)_2$ and 15 mM ethylene glycol-bis(2-aminoethylether)-N, N,N′,N′-tetraacetic acid (EGTA). Electrodes were filled with 3 M KCl and had resistances of 0.3–1.0 MΩ. Recordings were conducted at room temperature from a holding potential of −90 mV. Leak currents were subtracted using a P/4 protocol.

Whole-cell Patch-clamp electrophysiology

HEK293 cells were transfected (in 35-mmdiameter wells) with Lipofectamine 2000 (Invitrogen, Carlsbad, CA, USA) and plated onto coverslips coated with Matrigel (BD Biosciences, San Diego, CA, USA).

Cells were transfected using a total of 4.4 μg DNA having a ratio by weight of 2:1.6:0.4:0.4 of $Ca_V\alpha_1$:$Ca_V\beta_{2a}$:$Ca_V\alpha_2\delta$-1:sv40 T-antigen plasmids. The SV40 T-antigen plasmid was used to increase channel expression. Transfected cells were identified visually using an enhanced green fluorescent protein (EGFP) expression in the second cassette of the plasmid expressing the β_2a subunit. Whole cell patch clamp (Hamill et al., 1981) was used to record Ca^{2+} and Ba^{2+} currents at room temperature (23 ± 2°C) 48–72 h post-transfection. Data acquisition was performed using pCLAMP 9 (Molecular Devices, Sunnyvale, CA, USA) and an Axopatch 200B amplifier (Molecular Devices). Pipettes were pulled from borosilicate glass capillaries (TW150F-3; World Precision instruments, Sarasota, FL, USA) and polished (MF-900 microforge; Narishige, Tokyo, Japan) to obtain 2–3 MΩ resistances. Sixty to eighty percent of the voltage error due to the series resistance was compensated, and leak currents were subtracted using a P/4 protocol. For $Ca_V1.2$ and $Ca_V1.3$ experiments, the pipette solution contained 120 mM NMDG-Cl, 1 mM $MgCl_2$, 5 mM EGTA, 4 mM Mg-ATP, 42 mM HEPES (pH 7.3 adjusted with Methane sulfonic acid). Bath solution contained 40 mM $CaCl_2$ or 40 mM $BaCl_2$, 1 mM $MgCl_2$, 105 mM Tris (pH 7.3 adjusted with Methane sulfonic acid). For $Ca_V2.1$ experiments, the pipette solution contained 120 mM NMDG-Cl, 1 mM $MgCl_2$, 0.5 mM EGTA, 2 mM Mg-ATP, 60 mM HEPES (pH 7.3 adjusted with Methane sulfonic acid). Bath solution contained 10 mM $CaCl_2$ or 10 mM $BaCl_2$, 1 mM $MgCl_2$, 150 mM Tris (pH 7.3 adjusted with Methane sulfonic acid).

Single-channel recordings

HEK cells were maintained and transfected as described above. Cell-attached configuration of the patch clamp technique (Hamill et al., 1981) was used to record Ba^{2+} currents from single or multiple $Ca_V1.2$ channels at room temperature (23 ± 2°C) 48–72 h post-transfection. Data acquisition was performed using pCLAMP 9 (Molecular Devices, Sunnyvale, CA, USA) and an Axopatch 200B amplifier (Molecular Devices). Pipettes were pulled from quartz glass capillaries (QF100-70-7.5; Sutter Instrument, Novato, CA, USA) using a Laser-Based Micropipette puller (P-2000, Sutter Instrument, Novato, CA, USA), and filled with 140 mM TEA-Cl, 40 mM $BaCl_2$, 10 mM HEPES (pH 7.4 adjusted with TEA-OH). To zero membrane potential, the bath solution contained 132 mM K glutamate, 5 mM KCl, 5 mM NaCl, 3 mM $MgCl_2$, 2 mM EGTA, 10 mM glucose, 20 mM HEPES (pH 7.4 adjusted with KOH) (Dick et al., 2016). Recordings were low pass filtered with a cutoff frequency of 2 kHz and digitized at 50 ms. Patches were stimulated by a voltage ramp from −80 mV to 50 mV over the duration of 200 ms. The leak for each trace was subtracted using a linear fit added to an exponential fit.

Data Analysis

All results are from at least two independent oocyte batches or at least two independent transfections. Data were analyzed with Clampfit 10.6 (Axon Instruments). Activation curves were obtained by fitting the data with the following Boltzmann equation: $I/I_{max} = 1/(1+\exp((V_{0.5}-V_m)/k))$, where $V_{0.5}$ is the half-activation potential, V_m is the membrane potential, and k is the slope factor. Dose–response curves were calculated as follows: $I_x/I_{3nMCa^{2+}} = 1/(1 + x/IC_{50})$, where I_x is the current amplitude at the Ca^{2+} concentration x, $I_{3nMCa^{2+}}$ is the current amplitude at 3 nM and IC_{50} is the half-maximal inhibitory concentration. VDI time constant (τ_{inact}) was determined at a test potential of +20 mV using the formula $I = A \exp(-t/\tau) + C$, where I is the recorded current, A is the peak current, C is the residual current at steady state, and t is the time. Current density was determined as the ratio between current amplitude (pA) and the membrane capacitance (pF).

QUANTIFICATION AND STATISTICAL ANALYSIS

All the details of data analysis and statistical analysis can be found in the Method Details and figure/table legends. All data values are presented as mean ± SEM 'n' represents the number of cells. Statistical significance of the observed effects was assessed by Student's t test, using SigmaStat 3.1 software. $p < 0.01$ was considered significant, unless otherwise stated.

Neuron, Volume *101*

Supplemental Information

A Selectivity Filter Gate Controls Voltage-Gated Calcium Channel Calcium-Dependent Inactivation

Fayal Abderemane-Ali, Felix Findeisen, Nathan D. Rossen, and Daniel L. Minor Jr.

Supplementary material for

A selectivity filter gate controls voltage-gated calcium channel calcium-dependent inactivation

Fayal Abderemane-Ali[1], Felix Findeisen[1], Nathan D. Rossen[1], and Daniel L. Minor, Jr.[1-5**†]

[1]Cardiovascular Research Institute

[2]Departments of Biochemistry and Biophysics, and Cellular and Molecular Pharmacology

[3]California Institute for Quantitative Biomedical Research

[4]Kavli Institute for Fundamental Neuroscience

University of California, San Francisco, California 93858-2330 USA

[5]Molecular Biophysics and Integrated Bio-imaging Division

Lawrence Berkeley National Laboratory, Berkeley, CA 94720 USA

*Correspondence to: daniel.minor@ucsf.edu

[†]Lead contact

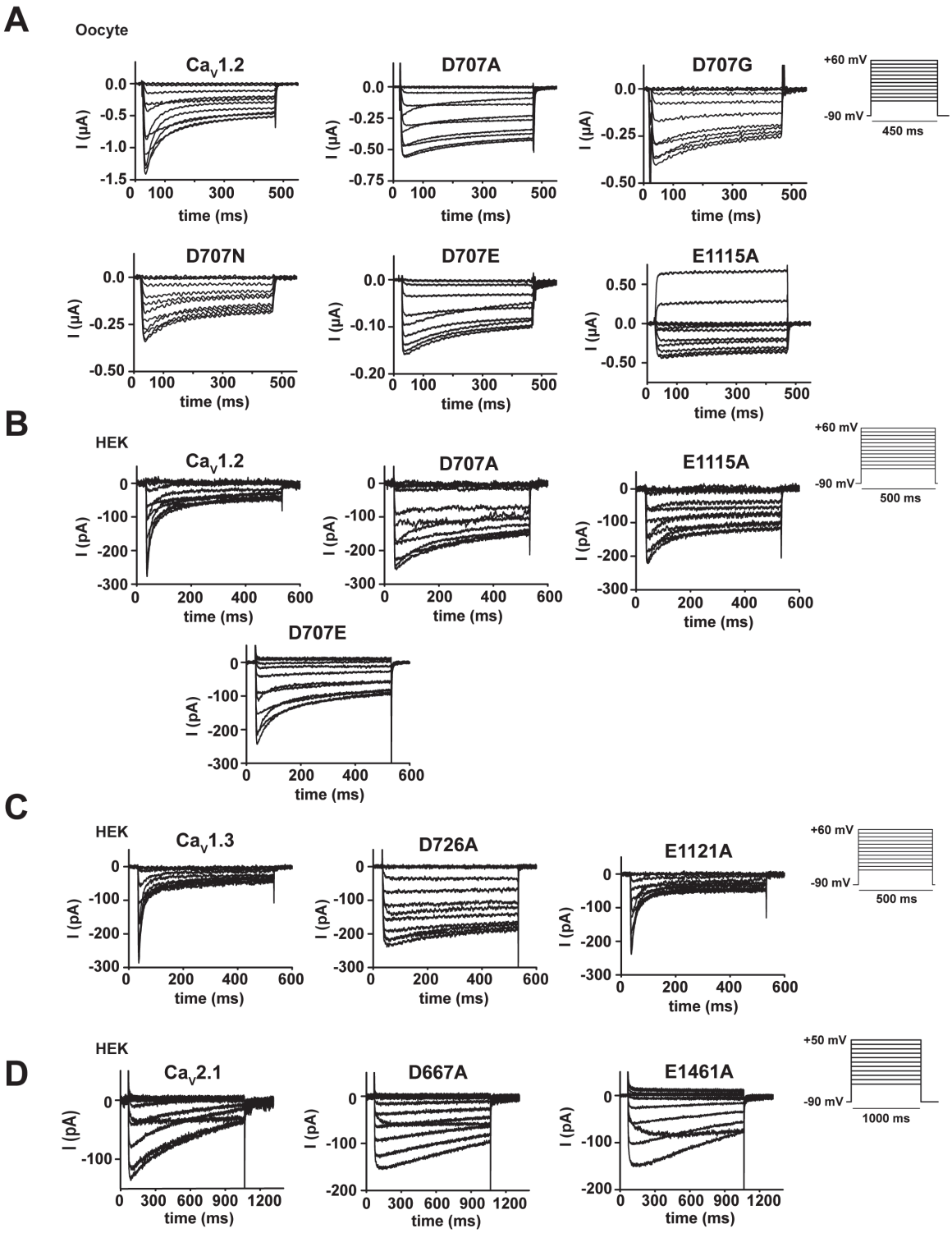

Figure S1 Exemplar Ca^{2+} currents for $Ca_V1.2$, $Ca_V1.3$, $Ca_V2.1$, and mutants co-expressed with $Ca_V\beta_{2a}$. Related to Figures 1, 2, and 4. Exemplar traces recorded in **A,** *Xenopus* oocytes expressing $Ca_V1.2$ or the indicated mutants, **B,** HEK 293 cells expressing Cav1.2 or the indicated mutants, **C,** HEK 293 cells expressing $Ca_V1.3$ or the indicated mutants, and **D,** HEK 293 cells expressing $Ca_V2.1$ or the indicated mutants. Currents were evoked using a multi-step activation protocol (insets).

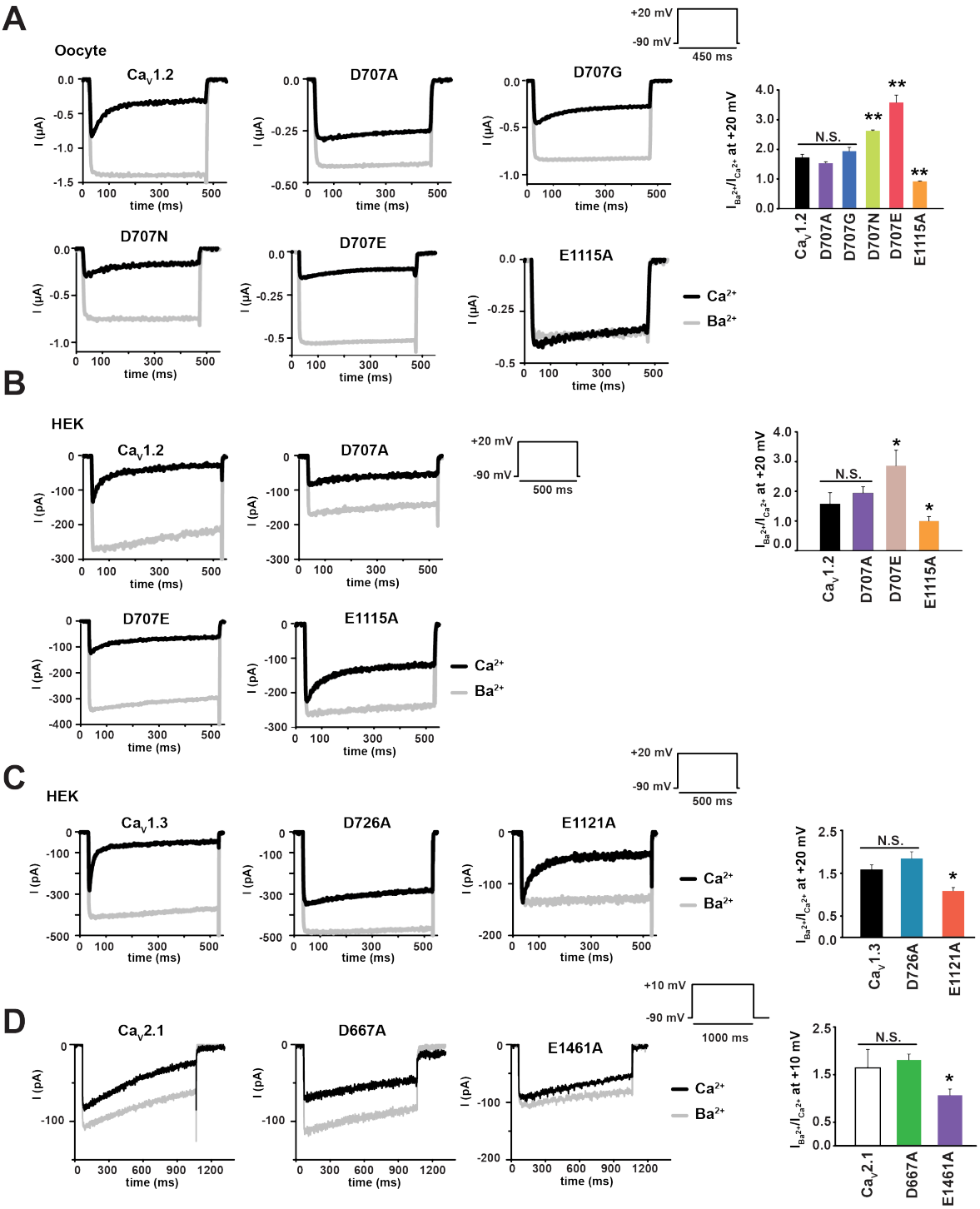

Figure S2 SFII (+1) mutants do not dramatically reduce Ca_V selectivity properties. Related to Figures 1, 2, and 4. A, Exemplar recordings at +20 mV in Ca^{2+} (black) or Ba^{2+} (grey) from *Xenopus* oocytes expressing $Ca_V1.2$ or indicated mutants, **B,** from HEK293 cells expressing $Ca_V1.2$ or indicated mutants, **C,** from HEK293 cells expressing $Ca_V1.3$ or indicated mutants, and **D,** HEK293 cells expressing $Ca_V2.1$ or indicated mutants. Right panels represent averaged values of ratios between Ba^{2+} and Ca^{2+} peak current amplitude at +20 mV or $Ca_V1.2$ and $Ca_V1.3$ or at +10 mV for $Ca_V2.1$. '*' indicates $p<0.01$, '**' indicates $p<0.001$, and 'N.S.' indicates 'not statistically significant' compared to wild-type channels. n values for all bar graphs are in Table 1. All recordings were made with $Ca_V\beta_{2a}$.

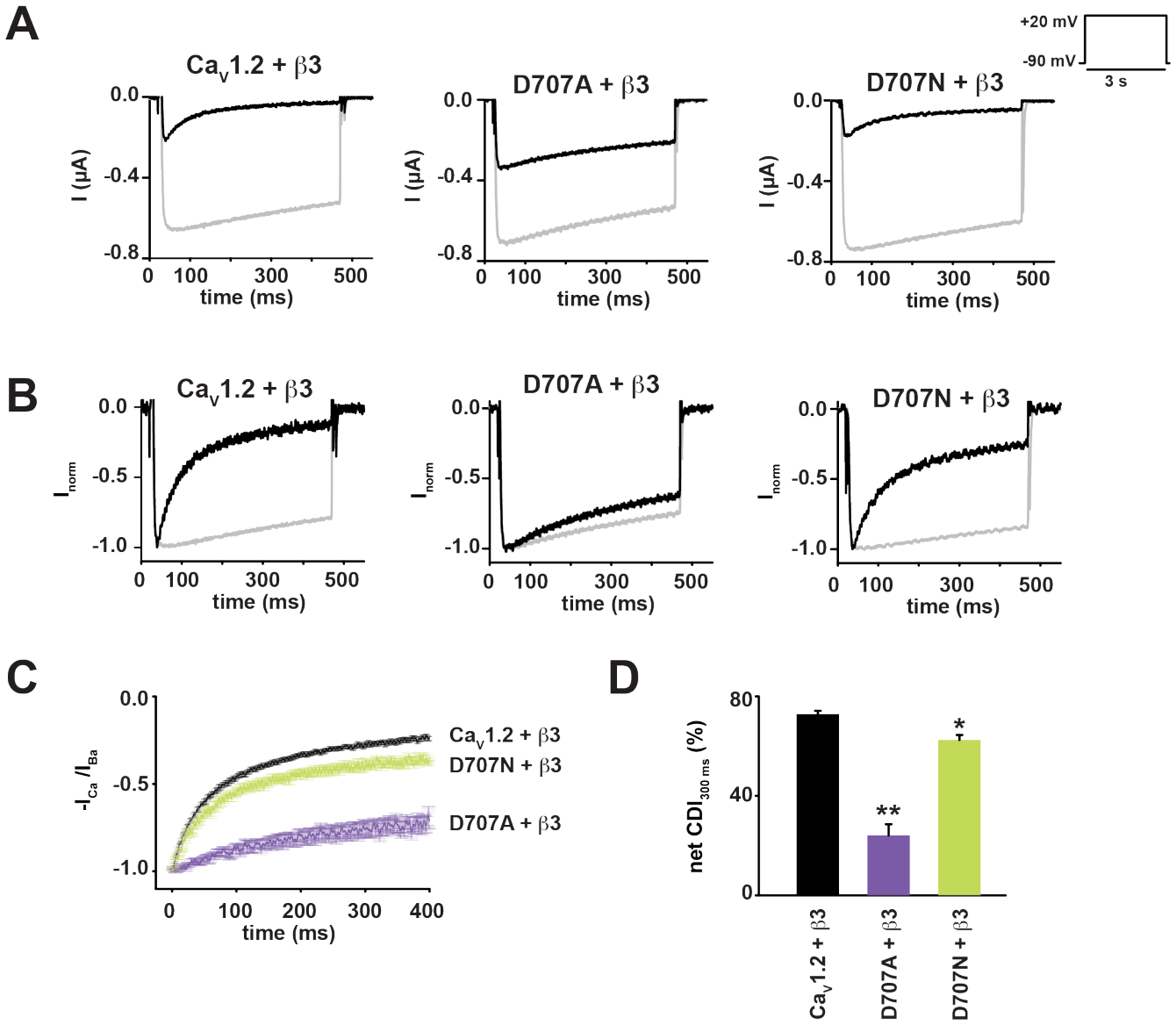

Figure S3 Ca$_V$1.2 selectivity filter mutations affect CDI independently of Ca$_V$β. Related to Figure 1. A, Exemplar raw traces recorded at +20 mV in Ca^{2+} (black) or Ba^{2+} (grey) from *Xenopus* oocytes expressing Ca$_V$1.2 or the indicated mutants with Ca$_V$β$_3$. **B,** Normalized traces from '**A**'. **C,** Ratio of normalized I_{Ca}/I_{Ba} currents (net CDI, (Barrett and Tsien, 2008; Findeisen and Minor, 2009)) showing average plots ± s.e.m. **D,** net CDI 300-ms post-depolarization. '*' indicates p<0.01 and '**' indicates p<0.001 compared to Cav1.2. n = 5-10.

Figure S4 Abderemane-Ali *et al.*

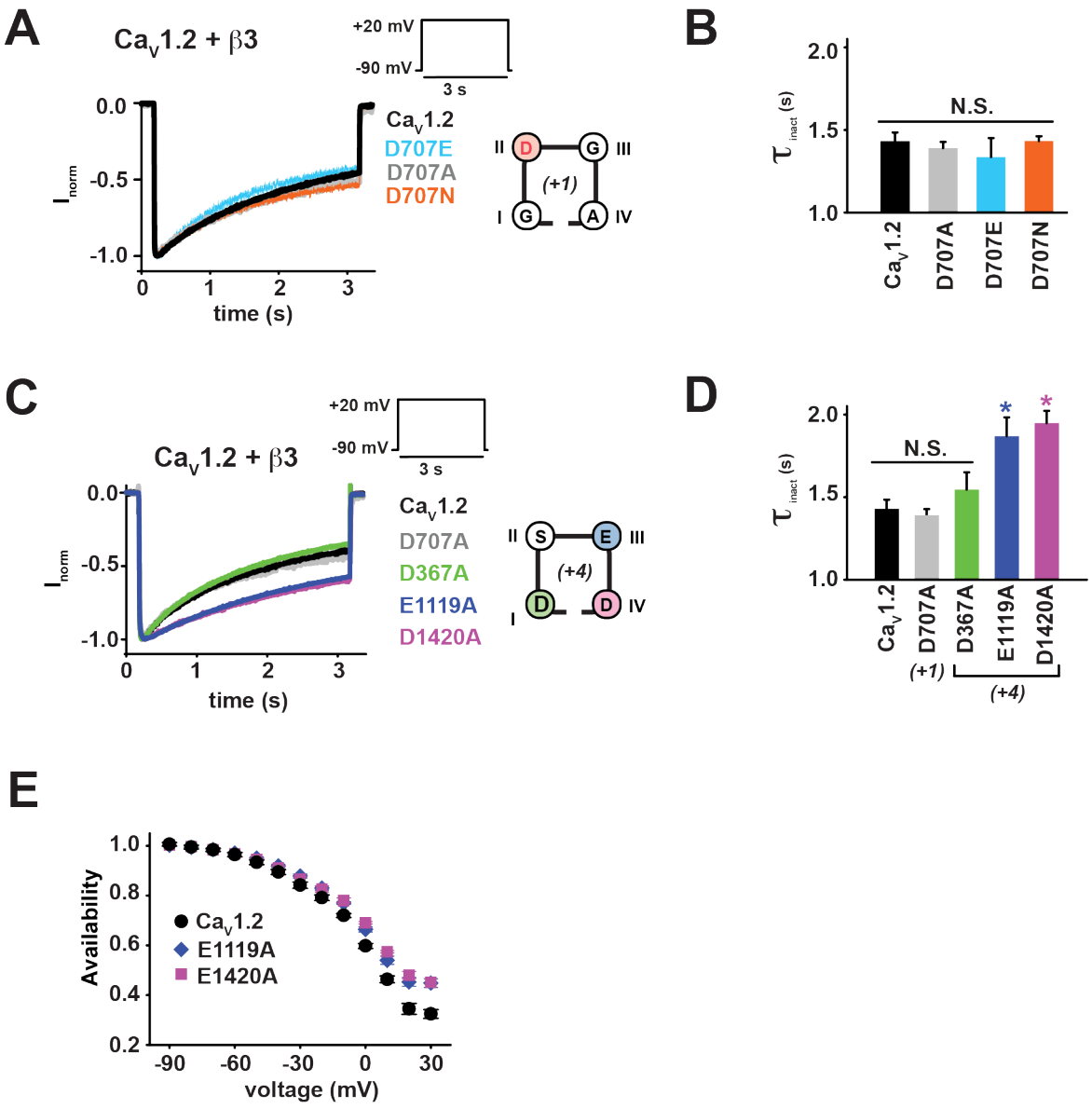

Figure S4 DII (+1) aspartate mutations affecting CDI spare VDI. Related to Figure 1. A, Exemplar two electrode voltage clamp recordings at +20 mV from *Xenopus* oocytes expressing $Ca_V1.2$ (black), $Ca_V1.2$ D707A (grey), Cav1.2 D707E (light blue), or Cav1.2 D707N (orange) with $Ca_V\beta_3$. **B,** τ inactivation (τ_{inact}) for '**A**'. n = 6-15. **C,** Exemplar two electrode voltage clamp recordings at +20 mV from *Xenopus* oocytes expressing $Ca_V1.2$ (black), $Ca_V1.2$ D707A (grey), Cav1.2 D367A (green), Cav1.2 E1119A (blue), or Cav1.2 D1420A (pink) with $Ca_V\beta_3$. **D,** τ inactivation (τ_{inact}) for '**C**'. n = 9-19. '*' indicates p<0.001, and 'N.S.' indicates 'not statistically significant' compared to $Ca_V1.2$. **E,** Voltage-dependent inactivation curves representing channel availability after a steady-state inactivation at the indicated potentials.

Figure S5 Abderemane-Ali *et al*.

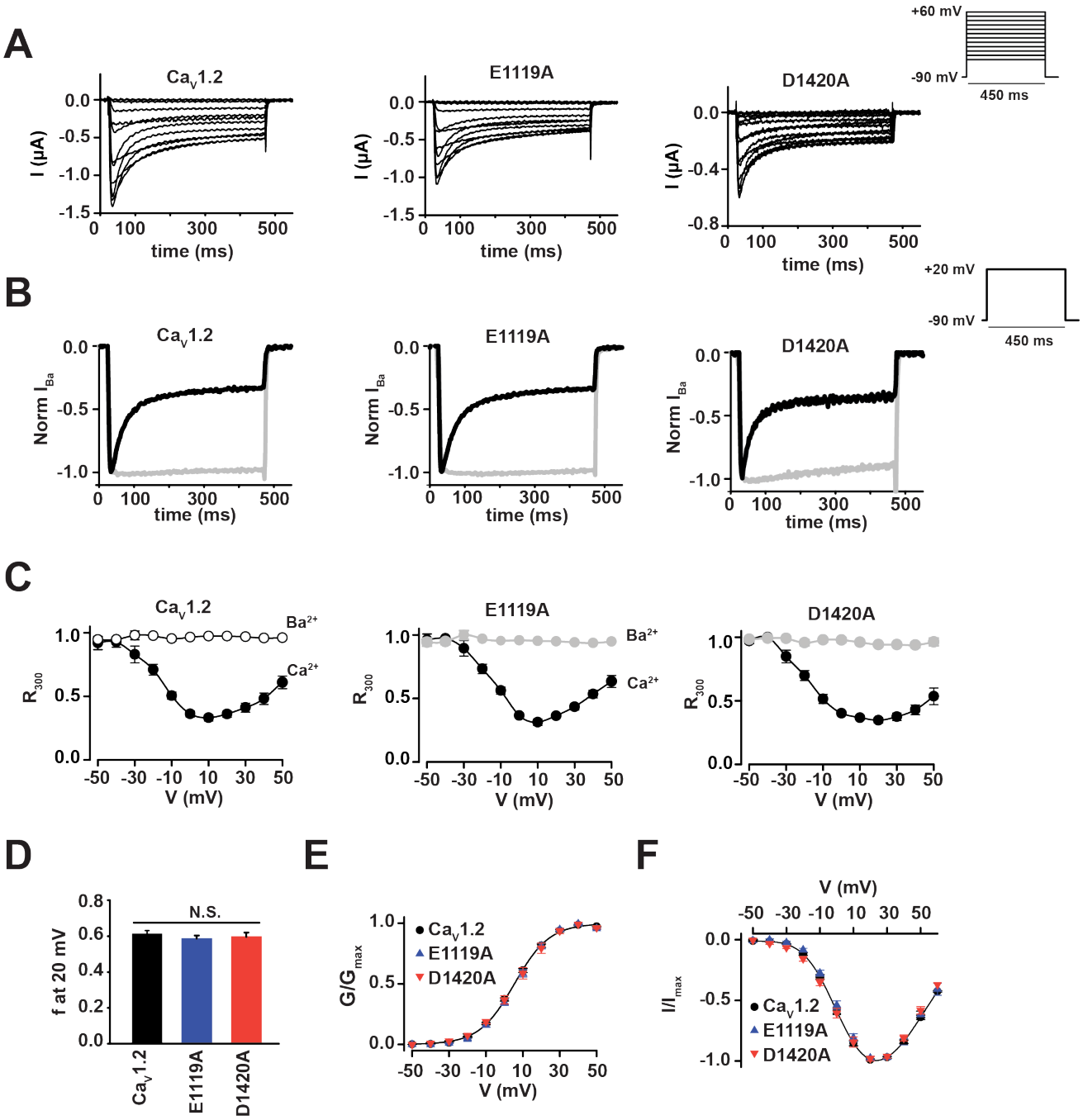

Figure S5 SF (+4) mutations affecting VDI spare CDI. Related to Figure 1. A, Exemplar traces recorded in *Xenopus* oocytes co-expressing $Ca_V1.2$, $Ca_V1.2$ E1119A, or Cav1.2 D1420A with $Cav\beta_{2a}$ in response to the indicated protocol. **B,** Exemplar normalized recordings at +20 mV in Ca^{2+} (black) or Ba^{2+} (grey) from *Xenopus* oocytes expressing $Ca_V1.2$, $Ca_V1.2$ E1119A, or Cav1.2 D1420A. **C,** Fractional current remaining 300 ms post-depolarization (R_{300}) as a function of the membrane potential for channels in '**B**'. **D,** Average fraction CDI (f) at +20 mV**.** 'N.S.' indicates 'not statistically significant'. n values are found in Table 1. **E,** Voltage-dependent activation curves for $Ca_V1.2$ (black circles), $Ca_V1.2$ E1119A (blue triangles), and Cav1.2 D1420A (red inverted triangles). **F**, I-V relationships for the indicated channels. Symbols are the same as '**E**'.

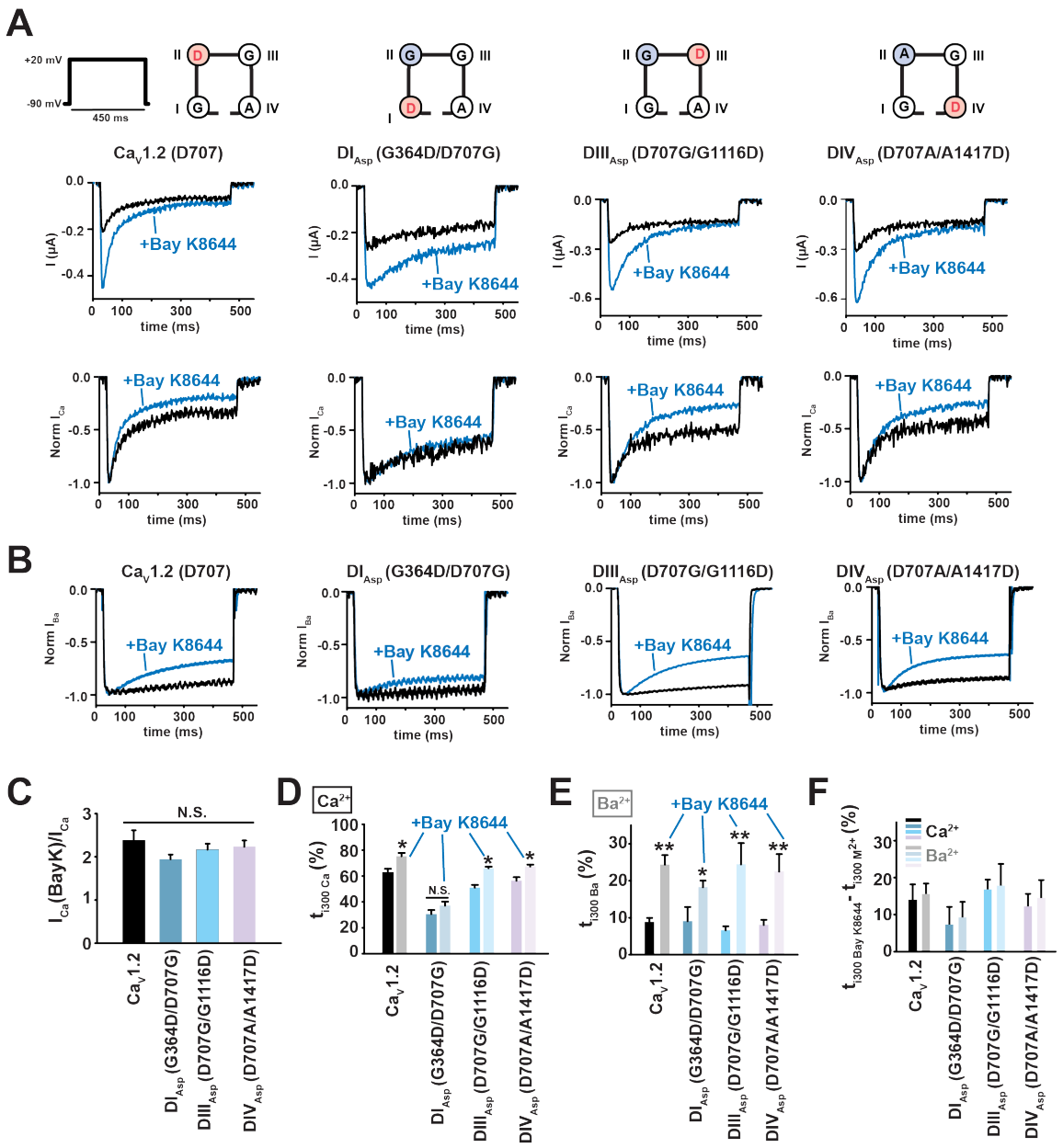

Figure S6 Ca$_V$1.2 CDI requires a negative charge at +1 position on DII, DIII, or DIV, not DI, regardless of the amount of Ca^{2+} influx. Related to Figures 3 and 5. A, Exemplar Ca^{2+} currents in response to a +20 mV depolarization from *Xenopus* oocytes, co-expressing Ca$_V$1.2 or the indicated mutants with Cavβ_{2a} in the absence (black) or presence of 5 μM Bay K8644 (blue). Raw traces (upper panels) and normalized traces (lower panels) are shown to illustrate Bay K8644 effects on both the peak current and inactivation, respectively. **B,** Exemplar normalized Ba^{2+} currents from *Xenopus* oocytes expressing Ca$_V$1.2 or the indicated mutants, in response to a +20 mV depolarization in absence (black) or in presence of 5 μM Bay K8644 (blue). **C,** Ratio of Ca^{2+} current amplitudes in presence, I$_{Ca}$(BayK), and in absence, I$_{Ca}$, of Bay K8644. 'N.S.' indicates not statistically different. n = 4-7. **D** and **E,** Percentage of inactivation 300 ms post-depolarization (t$_{i300}$) in the absence (dark bars) and presence of Bay K8644 (light bars) on recordings performed using **D**, Ca^{2+}, or **E**, Ba^{2+} as the charge carrier. '*' indicates p<0.01 and '**' indicates p<0.001. n= 6-11. **F,** Difference in t$_{i300}$ induced by Bay K8644 in Ca^{2+}(dark bars) and Ba^{2+} (light bars).